Chemical Geology 680 (2025) 122649

Contents lists available at ScienceDirect

Chemical Geology

journal homepage: www.elsevier.com/locate/chemgeo

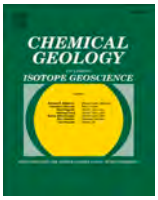

Carbonate metasomatism at mantle wedge conditions, evidence from trace element and stable isotope (Fe, Zn) signatures of orogenic peridotites

B. Debret [a,*], P.A. Sossi [b], N. Malaspina [c], A. Gautier [d,e], N. Mattielli [d], H. O'Neill [f], J. Villalobos-Orchard [a], F. Moynier [a]

[a] Université Paris Cité, Institut de physique du globe de Paris, CNRS, Paris, France
[b] Department of Earth Sciences, ETH Zürich, Zürich, Switzerland
[c] Dipartimento di Scienze dell'Ambiente e della Terra, Università degli Studi di Milano Bicocca, Milano, Italy
[d] Laboratoire G-Time, DGES, Université Libre de Bruxelles, ULB, Brussels, Belgium
[e] Laboratoire Magmas et Volcans, Université Clermont Auvergne, CNRS, IRD, OPGC, Clermont-Ferrand, France
[f] School of Earth, Atmosphere and Environment, Monash University, Melbourne, Australia

ARTICLE INFO

Editor: S Aulbach

Keywords:
Mantle wedge
Subduction zones
Stable isotopes
Peridotite
Metasomatism
Oxygen fugacity

ABSTRACT

The composition and redox state of the mantle wedge over geological time can be impacted by fluid transfer from the slab during subduction. Although arc magmas are oxidised and enriched in fluid-mobile elements relative to mid-ocean ridge basalts (MORB), the nature of the fluid phase (aqueous or melts) produced by the slab in mantle wedge remains debated. Here we compare the elemental and isotopic (Fe and Zn isotopes) composition of both unmetasomatised and metasomatized ultramafic rocks from the Western Alps, respectively the Balmuccia and Finero massifs, to identify and characterise the relative effects of subduction-related processes on mantle peridotite composition. The metasomatism of Finero massif is evidenced by Light Rare Earth Element (LREE), U and Th enrichment coupled with isotopically light Zn and Fe signatures and an increase in oxygen fugacity relative to the MORB mantle-like peridotites of the Balmuccia massif. Negative correlations between LREE/HREE and U/Th ratios in metasomatized samples suggest preferential transport of Th relative to U in the infiltrating phase. Based on experimental constraints on fluid/melt partitioning, these observations are most consistent with Th dissolution in slab-derived melts. On the other hand, the light Zn isotope signatures in the Finero peridotites relative to those of Balmuccia peridotites are inconsistent with metasomatism by silicate melts and melt extraction processes. Trace elements and Zn isotopes results can be reconciled through the metasomatism of the mantle wedge by carbonate bearing fluids or melts in an open system. This process favours the formation of isotopically light metasomatic minerals in the Finero peridotite and the subsequent release of isotopically heavy CO_2-rich fluids or melts, probably during massif exhumation.

1. Introduction

The chemical exchange occurring at subduction zones plays a major role in shaping the composition of the Earth's surface and its interior over geological timescales (e.g., Duncan and Dasgupta, 2017; Eguchi et al., 2020). During oceanic lithosphere burial, the metamorphic reactions caused by the increase of pressure and temperature (P-T) release fluids such as aqueous solutions, melts or supercritical liquids to the mantle wedge, ultimately resulting in the genesis of arc magmas. However, the nature of the mobile fluid phase(s) remains largely debated owing to the uncertainty over the chemical imprints they leave in the resulting products of arc magmatism (e.g., Morris et al., 1990; Johnson and Plank, 2000). Identifying the nature of these mobile fluids is therefore of critical importance, as they affect the elemental mobility between crustal and mantle reservoirs (Kessel et al., 2005), the development of major ore deposits and mass balance at the scale of the subduction zone.

Arc magmas are commonly enriched in fluid-mobile large-ion lithophile elements (LILE) and depleted in high field strength elements (HFSE), relative to mid-ocean ridge basalt (MORB; Pearce, 1982). These chemical features are generally reconciled in a three-component model, which includes the depleted mantle wedge, subducted sediments and

* Corresponding author.
E-mail address: debret@ipgp.fr (B. Debret).

https://doi.org/10.1016/j.chemgeo.2025.122649
Received 4 December 2024; Received in revised form 23 January 2025; Accepted 24 January 2025
Available online 25 January 2025

altered oceanic crust (AOC; e.g., Hawkesworth et al., 1993; Plank and Langmuir, 1993; Miller et al., 1994; Elliott et al., 1997; Class et al., 2000; Elliott, 2004). However, whether or not the slab-derived components are directly transferred to the mantle wedge by fluids or indirectly, through an intermediate reservoir (e.g., serpentinite melange; Marschall and Schumacher, 2012), and their nature (supercritical/liquid/fluid) remain an active research frontier. Orogenic suprasubduction mantle peridotites are an alternative and complementary way to arc magmas for studying fluid/melt crust-to-mantle transfer in subduction zones. Petro-geochemical reconstructions show that these rocks, from a diversity of localities, contain high-pressure volatile-bearing minerals (e.g., phlogopite, amphibole, carbonate and sulfide) and anhydrous (e.g., pyroxene, garnet) phases enriched in LILE and light rare earth elements (LREE) with respect to heavy rare earth elements (HREE; e.g., Zanetti et al., 1999; Nimis and Morten, 2000; Zhang et al., 2000, 2007; Malaspina et al., 2006, 2009; Scambelluri et al., 2006; Selverstone and Sharp, 2011; Chen et al., 2017; Förster et al., 2024). These geochemical features are characteristic of slab-derived components. However, the exact nature of the metasomatic agent able to transport the elemental budget at high pressure (HP) remains unclear as the orogenic peridotites often record multistage metamorphic events, including protolith inheritance, HP-metasomatism and late exhumation processes, leading to variable trace element signatures from one geodynamic setting to another. Hence it remains an open question as to whether the geochemical records of metasomatized orogenic peridotites correspond to heterogeneous conditions in the suprasubduction mantle wedge worldwide or whether these relate to complex and specific P-T paths associated with regional and multiple metasomatic events (e.g., Malaspina et al., 2006, 2023; Scambelluri et al., 2006; Zhang et al., 2007; Pellegrino et al., 2020).

Metal stable isotope variations have the potential to complement trace element observations in mantle wedge environments. This is because the formation of melts, aqueous and supercritical fluids or brines can lead to contrasting isotope fractionation of elements that are sensitive to the speciation of the fluid/liquid phase, such as Zn and Fe (e.g., Williams et al., 2004; Debret et al., 2016, 2021; Liu et al., 2016; Pons et al., 2016; Moynier et al., 2017; Wang et al., 2017; Gerrits et al., 2019; Sossi and Debret, 2021; Li et al., 2024). In addition to chemical composition, this fractionation is also influenced by the redox state of the fluid or melt, since equilibrium isotope fractionation between different fluids and minerals is driven by contrasts in bonding conditions between chemical elements, including coordination degree and oxidation state (Ducher et al., 2016; Fujii et al., 2014; Polyakov and Mineev, 2000; Schauble, 2004; Sossi and O'Neill, 2017). Iron isotopes in arc magmas are systematically lighter than their MORB counterparts at a given Mg # ($Mg/[Mg + Fe^{2+}]$) (Dauphas et al., 2009; Foden et al., 2018; Nebel et al., 2015; Yan et al., 2024), attesting to processes occurring in subduction zones that are distinct from those during the genesis of MORB. One proposed mechanism states that Fe is transported by slab-derived fluids, which is supported by the inverse correlation observed between the slab thermal parameter and the iron isotope composition of basaltic magmas from arcs worldwide (Foden et al., 2018). This is further supported by the sympathetic enrichment of B (relative to fluid-immobile Nb) in these lavas (Chen et al., 2023).

Another way of testing this hypothesis is through examination of the isotopic signature of metasomatized orogenic peridotites that provide complementary information on redox processes occurring in subduction zones. In detail, the direction and magnitude of the isotope fractionation of such metasomatized peridotites relative to those unaffected by subduction processes can provide insights into the nature of the fluid involved (i.e., melts, aqueous and supercritical fluids or brines) and the oxygen fugacity conditions in the mantle wedge. For example, Turner et al. (2018) reported light Fe isotope signature in peridotite xenoliths hosted in basaltic andesites on the Batan Island (Philippines) that are too light to have been formed by equilibrium partial melting alone. This requires the addition of slab fluid enriched in light Fe isotopes. Similarly, serpentinized forearc mantle wedge peridotites show large negative deviations (down to $\delta^{56}Fe = -0.26$ ‰; Debret et al., 2020) that are correlated with high bulk rock $Fe^{3+}/\sum Fe$ ratio, suggesting the transfer of oxidizing slab fluids with an isotopically light signature. Silicate melts are invariably heavier than the peridotites or eclogites from which they are derived owing to the greater incompatibility of Fe^{3+} relative to Fe^{2+} (Dauphas et al., 2009; Tiraboschi et al., 2023). Therefore, the isotopically light signatures observed in metasomatized peridotites are likely imparted by slab-derived fluids, in which ferrous iron, particularly in chloride form, is more soluble than ferric iron (e.g., Chou and Eugster, 1977).

To examine the nature of slab metasomatism and the oxygen fugacity (fO_2) record of mantle wedge peridotites, we combine trace element concentration with Fe and Zn isotope analyses in peridotites from Balmuccia and Finero (Ivrea Zone, Italian Alps). We show that metasomatized peridotites from Finero have high LREE/HREE relative to unmetasomatized samples from Balmuccia and are also 1 $\log_{10}$ unit more oxidised, which is consistent with the percolation of slab-derived fluids. A negative correlation between U/Th and LREE/HREE ratios is associated with isotopically light Zn signature and high Zr/Hf ratios in metasomatized samples, which cannot be achieved through simple metasomatism of peridotites by silicate melts (or fluids) at high pressures and temperatures. Rather, these constraints suggest the dissociation of an oxidised, carbonate rich metasomatic agent (either fluid or melt) probably during Finero massif exhumation.

2. Geological settings

Balmuccia and Finero massifs are the largest and most extensively studied ultramafic bodies outcropping in the northern part of the Ivrea Zone (Fig. 1a). These bodies are aligned at the northwestern margin of the lowest stratigraphic units of the Ivrea Zone, representing the lowermost unit of the alpine continental crust (Fountain, 1976; Mehnert, 1975). Both Balmuccia and Finero massifs were tectonically emplaced into the Ivrea crust during the Alpine Orogeny (Lu et al., 1997;

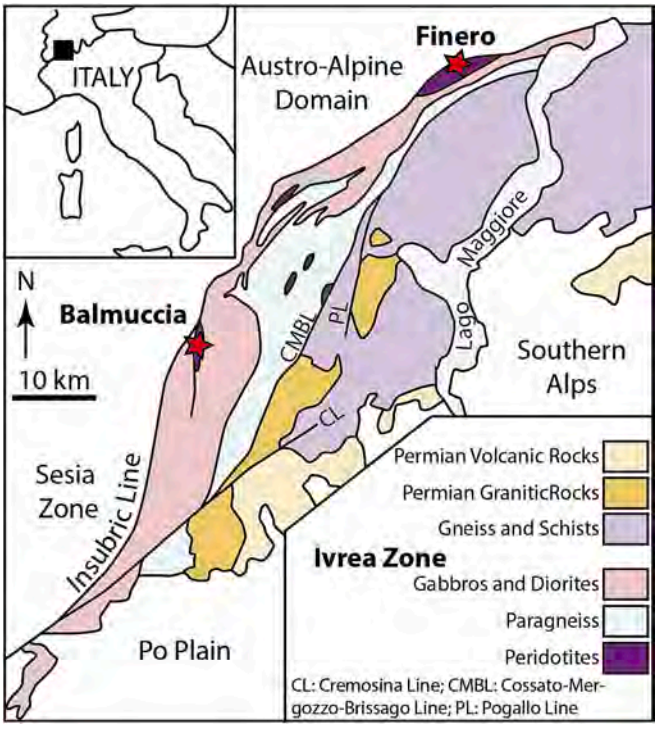

Fig. 1. Generalized geologic maps of the Ivrea- zone (northern Italy). The red stars correspond to the studied ultramafic massifs. (For interpretation of the references to colour in this figure legend, the reader is referred to the web version of this article.)

Quick et al., 1995). Despite their similar tectonic locations, these massifs display strong petrological and geochemical differences suggesting that they represent different segments of the lithosphere, generated in different tectonic environments (Rivalenti and Mazzucchelli, 2000; Selverstone and Sharp, 2011).

The Balmuccia ultramafic massif is a 5 km-long lens bounded by the Lensch mafic complex. The massif is dominated by spinel lherzolite with minor harzburgite and dunite (associated with chromitites) often interlayered with pyroxenites, which occur in two series, the chrome diopside (Cr-Di) and the aluminium augite (Al-Aug) suites, and is crosscut by a wide range of later mafic dykes (Mazzucchelli et al., 2009; Shervais, 1979). The pyroxenites display Sr and Nd isotopic compositions similar to MORB and are indistinguishable from that of the host lherzolite, suggesting that the massif record a tectonic thinning of a subcontinental lithosphere prior the ocean formation (Shervais and Mukasa, 1991). The Balmuccia massif is characterized by extremely fresh peridotites and pyroxenites with negative loss-on-ignition values (Shervais, 1979; Shervais and Mukasa, 1991). The studied samples are taken from Sossi et al. (2018). They were collected along the Sesia river that bisects the massif at its southern tip. This sample suite is subdivided according to peridotite, including lherzolite, harzburgite and dunite, and pyroxenites (Cr-Di and Al-Aug) (Table 1).

The Finero ultramafic massif is an antiformal body that comprises phlogopite- and amphibole-bearing peridotites at its core. The massif is surrounded by amphibolite- to granulite facies layered metagabbros (Zanetti et al., 1999). The abundance of hydrous phases (amphibole and phlogopite) is highly variable at both outcrop and massif scale (Giovanardi et al., 2014). Rare carbonate (dolomite) were also described by Zanetti et al. (1999) and Morishita et al. (2008). In contrast to Balmuccia, spinel harzburgite is the dominant rock type within the peridotite, with subordinate lherzolite, dunite and websterite. They are often interlayered with clinopyroxenite. Although the nature of the metasomatic agent (i.e., melt, aqueous or supercritical fluids) is debated in detail, there is a general consensus that the phlogopite- and amphibole-bearing peridotites formed in a subduction-like context (Hartmann and Hans Wedepohl, 1993; Zanetti et al., 1999; Selverstone and Sharp, 2011). Based on bulk rock composition of phlogopite- and amphibole-bearing peridotites and thermodynamic modelling, Selverstone and Sharp (2011) calculated P-T conditions of equilibration nearby 900 °C and 1.2–1.6 GPa, compatible with shallow mantle wedge conditions. The studied samples were collected along the private road to the Finero quarry and along the Cannobino river, from the Provola bridge to the Creves–Cannobino confluence (Tommasi et al., 2017). We subdivided the studied samples according to their mineralogy, distinguishing between peridotites and pyroxenites (Table 1). The sampled peridotites correspond to spinel harzburgites with variable amounts of

Table 1
Fe and Zn isotope analyses in ‰.

Sample Name	Locality	Mineralogy	δ^{56}Fe	2sd	δ^{57}Fe	2sd	n	δ^{66}Zn	2sd	δ^{68}Zn	2sd	n
Western Alps												
BM-12	Balmuccia	Lherzolite	0.02	0.01	0.03	0.02	2	0.15	0.02	0.27	0.06	2
BM-14	Balmuccia	Lherzolite	0.06	0.01	0.10	0.01	2	0.16	0.06	0.31	0.12	1
BM19	Balmuccia	Dunite	0.04	0.01	0.06	0.02	2	0.12	0.02	0.23	0.04	2
BM22	Balmuccia	Lherzolite	0.03	0.02	0.04	0.03	2	0.18	0.06	0.37	0.08	2
BM-23	Balmuccia	Lherzolite	0.03	0.04	0.04	0.06	2	0.14	0.02	0.29	0.15	2
BM-26B	Balmuccia	Lherzolite	−0.04	0.01	−0.06	0.01	2	0.11	0.06	0.60	0.12	1
BM-27	Balmuccia	Lherzolite	0.01	0.04	0.01	0.06	6	0.14	0.04	0.28	0.09	2
BM28-Pd	Balmuccia	Dunite	0.01	0.01	0.02	0.02	2	n.d.		n.d.		
BM29-Pd	Balmuccia	Al-Aug	n.d.		n.d.			0.10	0.06	0.20	0.12	1
BM30	Balmuccia	Lherzolite	0.00	0.03	0.01	0.04	2	0.15	0.06	0.30	0.12	1
BM31	Balmuccia	Dunite	−0.03	0.02	−0.04	0.04	4	0.16	0.04	0.33	0.08	1
BM35	Balmuccia	Lherzolite	0.03	0.02	0.05	0.03	4	0.12	0.06	0.25	0.12	1
BM-40	Balmuccia	Lherzolite	0.03	0.03	0.05	0.05	2	0.12	0.02	0.26	0.04	2
BM42	Balmuccia	Lherzolite	n.d.		n.d.			0.16	0.06	0.30	0.12	1
BMH-1	Balmuccia	Lherzolite	0.00	0.00	0.00	0.00	2	0.18	0.06	0.39	0.12	1
BMH-2	Balmuccia	Lherzolite	0.03	0.01	0.05	0.02	2	0.13	0.11	0.25	0.23	2
BMH-3Pd	Balmuccia	Lherzolite	−0.01	0.02	−0.02	0.03	2	0.11	0.06	0.22	0.03	2
BMH-5	Balmuccia	Lherzolite	0.02	0.01	0.03	0.02	2	0.12	0.06	0.25	0.12	1
BMH-9	Balmuccia	Lherzolite	0.03	0.02	0.04	0.03	2	0.16	0.06	0.33	0.12	1
BM28-Px	Balmuccia	Clinopyroxenite	0.13	0.01	0.19	0.02	2	0.21	0.06	0.42	0.12	1
BM29-Px	Balmuccia	Clinopyroxenite	n.d.		n.d.			0.18	0.06	0.37	0.12	1
BMH-3Px	Balmuccia	Clinopyroxenite	0.09	0.01	0.13	0.01	2	0.23	0.01	0.45	0.01	2
FIN12	Finero	Serpentinite	0.08	0.09	0.13	0.11	4	n.d.		n.d.		
FIN2	Finero	Amp-Sp Harzburgite	−0.06	0.06	−0.09	0.14	3	−0.01	0.05	0.01	0.16	3
FIN3	Finero	Sp Harzburgite	0.00	0.03	−0.02	0.05	3	−0.21	0.03	−0.31	0.12	3
FIN4	Finero	Amp-Sp Harzburgite	0.00	0.03	0.01	0.07	2	0.14	0.03	0.30	0.14	5
FIN5	Finero	Phl-Sp Harzburgite	0.02	0.04	0.05	0.07	3	0.00	0.02	0.07	0.02	5
FIN6	Finero	Amp-Sp Harzburgite	0.01	0.04	−0.01	0.04	5	−0.07	0.04	−0.11	0.11	4
FIN8	Finero	Phl-Sp Harzburgite	−0.04	0.06	−0.07	0.07	2	−0.26	0.05	−0.33	0.10	3
FIN9	Finero	Amp-Sp Harzburgite	−0.04	0.00	−0.06	0.01	2	−0.01	0.02	0.10	0.07	5
FIN10	Finero	Amp-Sp Harzburgite	−0.01	0.01	0.00	0.03	4	−0.19	0.07	−0.28	0.15	2
FIN11	Finero	Clinopyroxenite	0.12	0.04	0.16	0.06	3	0.23	0.03	0.50	0.05	5
FIN7	Finero	Phl Clinopyroxenite	0.08	0.02	0.10	0.06	3	0.08	0.04	0.26	0.12	4
Standards												
BCR-2			n.d.		n.d.		–	0.15	0.04	0.31	0.08	5
Preferred values[1]								*0.17*	*0.05*			
BHVO-2			0.10	0.01	0.20	0.06	2	0.33	0.04	0.60	0.07	2
duplicate								0.31	0.02	0.55	0.07	
Preferred values[2]			*0.10*	*0.03*	*0.13*	*0.05*		*0.28*	*0.04*			
UB-N			0.03	0.04	0.07	0.07	3	0.29	0.07	0.59	0.13	3
Preferred values[3]			*0.06*	*0.03*	*0.08*	*0.05*		*0.38*	*0.09*	*0.73*	*0.3*	

1, Moynier et al. (2017); 2, Craddock et al. (2013); Telus et al. (2012)
Data for Balmuccia samples were reported in Sossi et al. (2016) (Fe) and Sossi et al. (2018) (Zn). When n = 1, the 2sd corresponds to long-term reproducibility.

clinopyroxene (< 10 %). The clinopyroxenes are often associated with large amount of fluid and mineral inclusions, such as olivine and orthopyroxene (Fig. 2a) suggesting a refertilization of the peridotite through metasomatic fluids. Amphibole and phlogopite are the dominant hydrous minerals (Fig. 2b).

3. Method

3.1. Mineral major element analyses

The major element composition (SiO_2, Al_2O_3, FeO_{Total}, MnO, MgO, CaO, Na_2O, K_2O, TiO_2) of spinels, olivines and orthopyroxenes from Finero massif was analyzed on a CAMECA SX100 electron microprobe at the Laboratoire Magmas et Volcans (Clermont-Ferrand, France) for oxygen fugacity estimates (see discussion). Quantitative analyses were performed using a monochromatic crystal filtering the polychromatic incident X-ray beam. For most analyses, the beam voltage was 15 kV and the intensity 15 nA. Results are displayed in Supplementary Table 1.

3.2. Bulk rock major element analyses

Major element analyses of Balmuccia ultramafic rocks are from Sossi et al. (2018).Major element analyses (SiO_2, Al_2O_3, Fe_2O_3, MnO, MgO, CaO, Na_2O, K_2O, TiO_2) of Finero ultramafic rocks were carried out at the Service of Analyses of Rocks and Minerals (SARM) in Nancy, France, using a Thermo Scientific iCap6500 ICP-OES. Sample digestions were performed on $LiBO_2$ fluxed fusions following the procedures described by Carignan et al. (2001). Results for reference material UB-N analyzed alongside the samples show a difference of less than 2 % with literature values (Supplementary Table 2).

3.3. Bulk rock trace element analyses

For trace element analyses of the Balmuccia samples, 100 mg of fine powder (crushed in a steel jaw crusher and ground in W—C mills) was dissolved on a hot plate in a concentrated HCl-HF-HNO3 (1:0.5:0.2) acid mixture at 140 °C for 2 days. During subsequent evaporation, 15.7 M HNO3 was added periodically to convert the residue to nitrates and avoid the formation of fluorides, which were then re-dissolved in 2 mL of 15.7 M HNO3 with a few drops of 24 M HF. The Teflon beakers containing the solutions were placed in a PTFE Teflon-lined high-pressure bomb vessel and heated to 200–210 °C in order to dissolve chromite. After drying down, they were re-dissolved in 2 mL of 15.7 M HNO3. Typically, 50 µL of this solution was diluted 100×, to 5 mL, with 2 % (0.317 M) HNO_3 and spiked with 10 ppb each of Rh and Re, resulting in a total dilution factor of ≈ 1000× (Eggins et al., 1997). Calibration was performed by standardization against synthetic solutions diluted to the 500, 100, 10, 1, and 0.1 ppb levels. These solutions were used in conjunction with BHVO-2 to correct for differences in the matrix between samples and the standard solutions, as well as oxide corrections on the Rare Earth Elements (REE). Rhodium (< 138 amu) and Re (≥ 138 amu) internal standards corrected were used for mass bias and instrumental drift corrections. Samples were introduced by a glass nebulizer to a Peltier-cooled glass spray chamber coupled to an Agilent 7700 quadrupole ICP-MS at the Australian National University. Collision/reaction cell gases were not used. Detection limits were of the order of 0.1 ppt (0.1 ppb in the original powder) and the relative standard deviation was typically between 0.1 and 2 % and did not exceed 5 %.

Additional, trace element data on Finero ultramafic rocks were carried out at the Institut de Physique du Globe de Paris (IPGP) using an Agilent 7900 quadrupole ICP-MS. Elements with masses between that of sodium (23) and arsenic (75), as well as silver (107), cadmium (111) and gadolinium (157), were measured using a collision-reaction cell with helium gas (5 mL/min) to remove polyatomic interferences. All other elements were measured without collision gas. Reported uncertainties were calculated using error propagation equations and considering the combination of standard deviation on replicated consecutive signal acquisitions ($n = 3$), internal-standard ratio and blank subtraction. A JP1 peridotite and a UB-N serpentinite were used as external standard. The obtained values are in good agreement with literature data (Supplementary Table 2).

3.4. Bulk rock Fe and Zn stable isotope analyses

50 mg of whole rock powders from the Finero massif were dissolved using concentrated HF and HCl acids in 7 mL PTFE Teflon square digestion vessels with wrench top closures in an oven at 160 °C for 3 days. The prior study of Debret et al. (2018) compared this method to Parr bomb dissolution techniques and showed that it results in the digestion of refractory phases, such as spinels, present in peridotites. Following evaporation of the HF and HCl, the samples were subsequently treated with a 1:3 mix of concentrated HCl and HNO_3 and refluxed at 140 °C for 3 days in an oven. Finally, samples were brought into solution in 6 M HCl prior to column chemistry. Quantitative

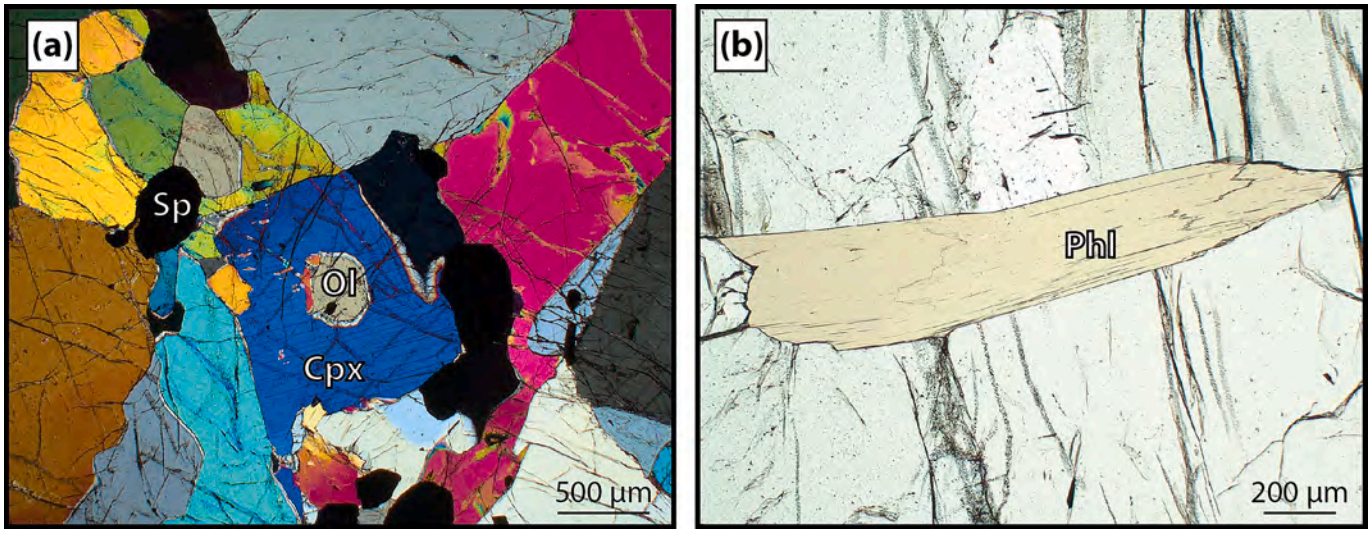

Fig. 2. Thin section microphotographs of the Finero peridotites. (a) Microphotograph (cross polarized light) of a clinopyroxene containing a large olivine cluster. This micro-texture indicates a reaction between olivine and a fluid / melt to form clinopyroxene. (b) Microphotograph (plane polarized light) of a phlogopite observed in Finero peridotites.

purification of Zn and Fe was achieved by chromatographic exchange, using 1 mL of AG1-x8 (200–400 mesh) and 1.2 mL Bio-Spin© Chromatography columns, following the procedure adapted from Maréchal et al. (1999) and developed by Sossi et al. (2015). All reagents used in the chemistry and mass spectrometry procedures were distilled and sub-boiled at the IPGP. The total procedural blank contribution was <18 ng for Zn and < 80 ng of Fe, which is negligible compared to the amount of Zn and Fe in the samples (blank contribution is <1 %).

Iron and zinc isotope analyses were performed by multiple-collector inductively-coupled-plasma mass-spectrometry (MC-ICP-MS; Thermo Scientific Neptune Plus) at the IPGP. Instrumental mass fractionation was corrected using the sample-standard bracketing technique. In the case of Fe analyses, solutions consisted of 3 ppm of natural Fe in 0.5 M HNO_3, which were introduced into the mass spectrometer using a quartz cyclonic spray chamber and PFA 100 μl/min nebulizer. The international Fe isotope standard IRMM-014 was used as both the bracketing and delta notation reporting standard. To resolve the polyatomic interferences $^{40}Ar^{16}O$, $^{+}\ ^{40}Ar^{14}N$, and $^{40}Ar^{16}OH^{+}$ that occur on masses ^{56}Fe, ^{54}Fe, and ^{57}Fe, respectively, the instrument was run in high-resolution mode, which gave a mass resolving power (mass/Δmass) of ~12,000. The standard Fe beam intensities typically varied between 15 and 20 V for ^{56}Fe using a 10^{10} Ω resistor. Data were collected in 15 cycles of 8.388 s integrations. Isotope ratios are reported as $\delta^{56}Fe$ in permil notation relative to IRMM-014 external standard:

$$\delta^{56}Fe = \left(\left({}^{56}Fe/{}^{54}Fe_{sample}\right)/\left({}^{56}Fe/{}^{54}Fe_{IRMM} - 1\right)\right) \text{ x } 1000$$

$$\delta^{57}Fe = \left(\left({}^{57}Fe/{}^{54}Fe_{sample}\right)/\left({}^{57}Fe/{}^{54}Fe_{IRMM} - 1\right)\right) \text{ x } 1000$$

The $\delta^{57}Fe$ was given to demonstrate mass dependency of the measurements. All reported errors are 2SD. Mass dependence, long-term reproducibility, and accuracy were evaluated by analyzing an in-house $FeCl_2^-$ salt standard. The values obtained for repeated measurements of this standard solution yielded average $\delta^{56}Fe$ values of −0.75 ± 0.04 ‰ and $\delta^{57}Fe$ values of −1.12 ± 0.13 ‰ 2sd, n = 21. These average values are in excellent agreement with previous measurements (Williams and Bizimis, 2014). The international rock reference materials United States Geological Survey (USGS) BCR-2 (basalt), USGC PCC-1 (peridotite) and Centre de Recherches Pétrographiques et Géochimiques (CRPG, Nancy, France) UB-N (serpentinite) were analyzed in the same analytical sessions as the samples, yielding $\delta^{56}Fe$ and $\delta^{57}Fe$ values in good agreement with literature values (Table 1). Iron isotope analyses for the Balmuccia peridotites are taken from Sossi et al. (2016) using the procedures described in Sossi et al. (2015).

Zinc isotope compositions were measured on the purified sample solutions. These solutions were prepared at 200 ng/g of natural Zn. This gave a Zn intensity of ~4 V for ^{64}Zn. The solutions were introduced to the instrument using a PFA 100 μl/min nebulizer coupled to a quartz cyclonic spray chamber. Owing to a lack of polyatomic interferences across the mass range for Zn the machine was operated in low mass resolution mode. The intensity of ^{62}Ni was monitored to correct for the potential interference of ^{64}Ni on ^{64}Zn. The Zn isotope composition of the sample is presented as a delta value in permil notation relative to the JMC-Lyon isotopic standard.

$$\delta^{66}Zn = \left(\left({}^{66}Zn/{}^{64}Zn_{sample}\right)/\left({}^{66}Zn/{}^{64}Zn_{JMC} - 1\right)\right) \text{ x } 1000$$

$$\delta^{68}Zn = \left(\left({}^{68}Zn/{}^{64}Zn_{sample}\right)/\left({}^{68}Zn/{}^{64}Zn_{JMC} - 1\right)\right) \text{ x } 1000$$

The $\delta^{68}Zn$ was given to demonstrate mass dependency of the measurements. Due to a limited supply of the JMC-Lyon standard solution, samples were measured relative to an AA-ETH pure Zn solution. Mass dependence, long-term reproducibility, and accuracy were evaluated by analyzing the JMC-Lyon standard solution in the same analytical sessions as the samples. The difference of AA-ETH relative to JMC-Lyon gave an average $\delta^{66}Zn$ value of +0.32 ± 0.04 ‰, 2sd, n = 18. This average value is in excellent agreement with previous measurements (Archer et al., 2017). The international rock reference materials USGS BCR-2 (basalt), BHVO-2 (basalt) and CRPG UB-N (serpentinite) were analyzed in the same analytical sessions as the samples, yielding $\delta^{66}Zn$ values in good agreement with literature (Table 1). Zinc isotope analyses for the Balmuccia peridotites are taken from Sossi et al. (2018) using the procedures described in Sossi et al. (2015).

4. Results

4.1. Major and trace elements

Results of whole rock analyses are reported in Supplementary Table 2 and illustrated in Figs. 3 and 4. Balmuccia peridotites are characterized by CaO, Al_2O_3 and MgO contents ranging from 0.20 to 7.21 wt%, 0.42 to 4.13 wt% and from 31.79 to 48.38 wt%, while pyroxenites are characterized by higher CaO (14.93–16.36 wt%), Al_2O_3 (4.50–12.24 wt %) and lower MgO (18.48–21.75 wt%) contents. All Balmuccia samples display mostly negative loss on ignition (L.O.I.) values (down to −0.39 wt% and up to 0.22 wt%), indicating weight gain during ignition due to oxidation of FeO to Fe_2O_3 and negligible loss of volatile compounds (H_2O, CO_2). Pyroxenites are characterized by high REE concentrations relative to peridotites but with a similar pattern. The REE patterns of Balmuccia ultramafic rocks display variable depletion in light REE (LREE; $La_N/Yb_N \leq 0.01–1$; N: chondrite normalized) and a flat medium and heavy rare earth element (M-HREE) segment. Their extended trace element patterns are characterized by a positive Pb anomaly (Pb_n/Ce_n = 6–212, n: primitive mantle normalized) and variable alkali enrichments (Cs_n/Th_n = 2–33) relative to neighbouring elements.

Finero peridotites display CaO, Al_2O_3 and MgO contents ranging from 0.20 to 4.13 wt%, from 0.19 to 1.51 wt% and from 38.16 to 45.93 wt%. The Finero pyroxenites are characterized by low CaO (3.74–16.24 wt%), Al_2O_3 (1.22–2.20 wt%) and high MgO (24.80–38.16 wt%) relative to Balmuccia pyroxenites. Finero samples are characterized by variable L.O.I. (b.d.l.-5.12 wt%), in agreement with the presence of hydrous phases in thin sections (amphibole or phlogopite, Fig. 2). One sample of serpentinite (FIN 12) display similar XMg (0.92), CaO (1.80 wt %) and Al_2O_3 (2.93 wt%) but high L.O.I. content (9.71 wt%) relative to fresh ultramafic rocks. The REE patterns are characterized by LREE enrichments (La_N/Yb_N = 1.4–11.5) and a variable Eu anomaly (Eu/Eu* = 0.8–2.2). As for Balmuccia, pyroxenites have similar patterns relative to peridotites but display higher REE concentrations. The extended trace element patterns are characterized by negative Zr, Hf (Hf_n/Sm_n < 1.1) and positive Sr (Sr/Sr* = 0.7–5.1) and Pb (Pb_n/Ce_n = 4–380) anomalies. They are also characterized by alkali (Cs_n/Th_n = 79–854) enrichments relative to neighbouring elements.

4.2. Fe and Zn isotopes

The $\delta^{66}Zn$ and $\delta^{56}Fe$ of Balmuccia ultramafic rocks range from +0.10 ± 0.06 to +0.23 ± 0.01 ‰ and from −0.04 ± 0.01 to +0.06 ± 0.01 ‰, respectively, and overlap those of the estimated compositions of the primitive mantle (Fig. 5). Balmuccia pyroxenites display high $\delta^{56}Fe$ values (from +0.09 ± 0.01 to +0.13 ± 0.01 ‰) and $\delta^{66}Zn$ values (from +0.18 ± 0.06 to +0.23 ± 0.01 ‰) relative to peridotites ($\delta^{56}Fe$ from −0.03 ± 0.02 to +0.06 ± 0.01 ‰; $\delta^{66}Zn$ from +0.10 ± 0.06 to +0.18 ± 0.06 ‰; (Sossi et al., 2018, Sossi et al., 2016). Finero peridotites display lower $\delta^{66}Zn$ and $\delta^{56}Fe$ values, from −0.26 ± 0.05 to +0.14 ± 0.03 ‰ and from −0.06 ± 0.05 to +0.06 ± 0.02 ‰, respectively (Fig. 5). Finero pyroxenites display high $\delta^{56}Fe$ (+0.08 ± 0.02 − +0.12 ± 0.04 ‰) and $\delta^{66}Zn$ (+0.08 ± 0.04 − +0.23 ± 0.03 ‰) values, similar to those of the Balmuccia pyroxenites.

5. Discussion

Mineralogical and geochemical variations affecting mantle peridotites are commonly interpreted to reflect variable degrees of melt

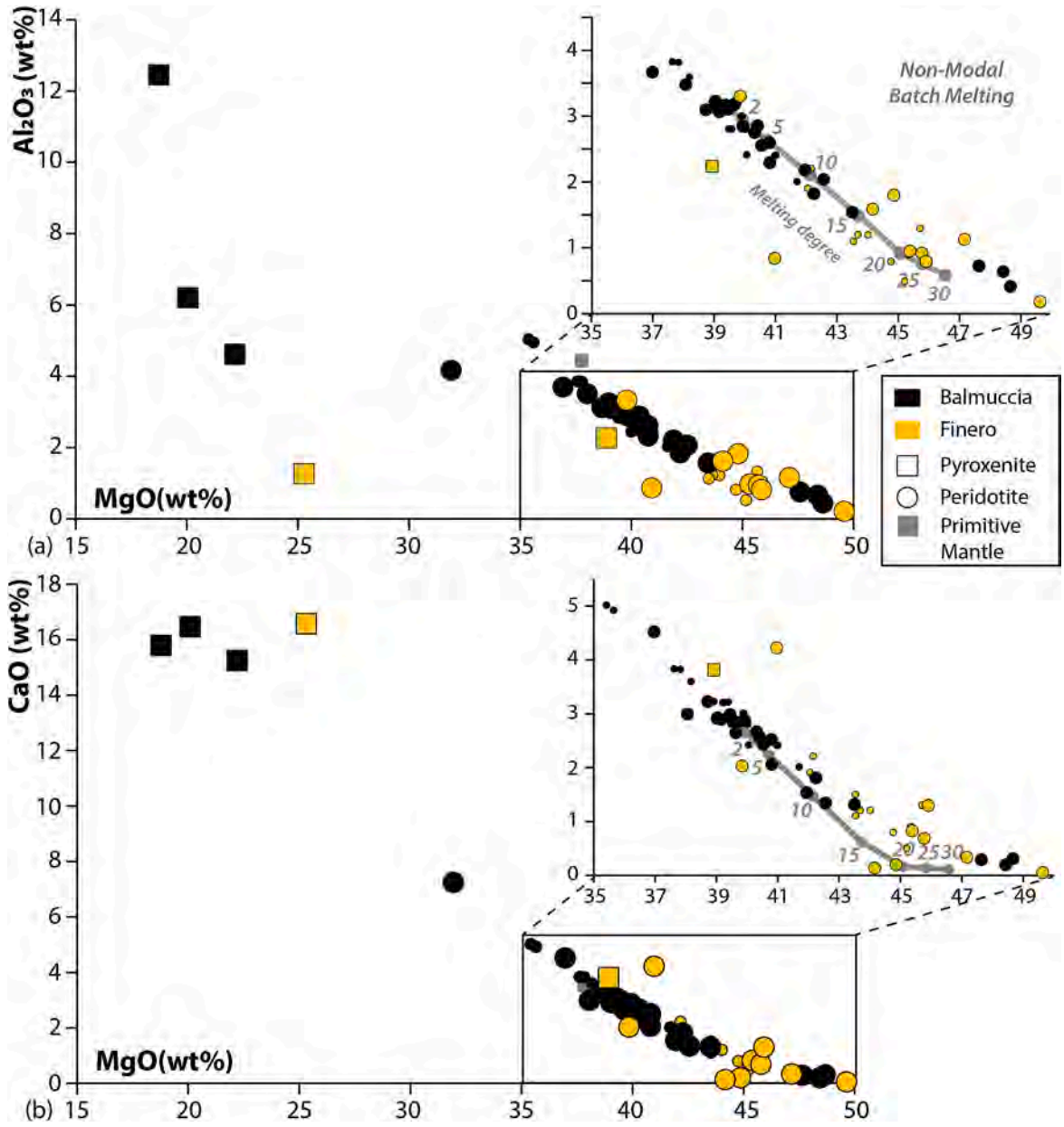

Fig. 3. Plots of (a) Al_2O_3 and (b) CaO versus MgO contents of Balmuccia and Finero samples (anhydrous contents in wt%). The boxes highlight a zoom in a small insert presenting peridotite data. Non-Modal batch melting model are shown in the small inserts, see main text and Supplementary Table 3 for more details about the model. Literature data are represented by small symbols (data from Hartmann and Wedepohl, 1993). Primitive mantle values are from McDonough and Sun (1995).

extraction that can be followed by either fluid- and/or melt metasomatism (e.g., Herzberg (2004) and reference therein). The Balmuccia ultramafic rocks correspond to fresh and unmetasomatised peridotites composed of clinopyroxene, orthopyroxene, olivine and spinel (Shervais and Mukasa, 1991; Hartmann and Hans Wedepohl, 1993). In contrast, the Finero samples contain high-pressure hydrous (i.e., amphibole, phlogopite) and carbon-bearing (i.e., dolomite) phases. Previous geochemical studies have proposed that these phases result from a high-pressure metasomatic event in a subduction related context (Cannaò et al., 2022; Giovanardi et al., 2014; Matsumoto et al., 2005; Selverstone and Sharp, 2011; Zanetti et al., 1999). This sample suite including both unmetasomatized and metasomatized ultramafic rocks therefore provides an unmatched opportunity to identify and characterise the relative effects of melting- and subduction related processes on the mantle wedge.

5.1. Partial melting of the mantle wedge

Before addressing the role of subduction-derived components in the studied samples, we first investigate the effects of high temperature melting processes on peridotite composition prior their metasomatism at high pressure. It must be noted that late alteration, e.g., serpentinization, can affect the δ^{66}Zn of peridotite, shifting them toward to heavy values relative to the primitive mantle (Debret et al., 2024). However, the Balmuccia samples are particularly fresh with Loss On Ignition values ranging from −0.4 to 0.2 wt%, while the Finero samples display low δ^{66}Zn relative to the primitive mantle. Similarly, no correlation between Zn (or Fe) isotopes and indices of serpentinization (e.g., LOI) was observed (Supplementary Fig. 1). We hence considered that the isotopic values of the samples are not primarily controlled by late alteration processes.

The “fertility” of a peridotite, which refers to the degree to which it

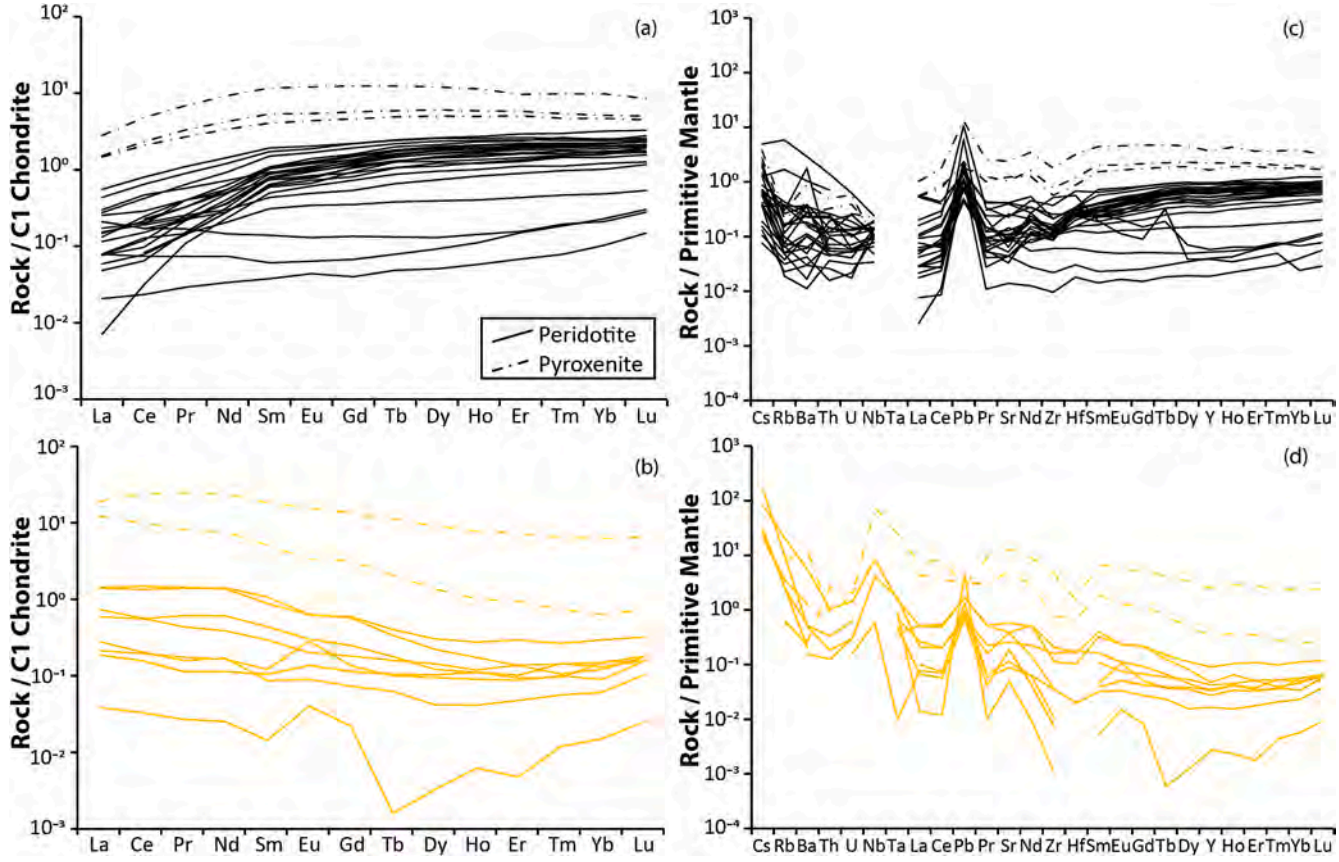

Fig. 4. Bulk rock REE and trace element patterns of (a, c) Balmuccia and (b, d) Finero ultramafic rocks normalized to the chondrite and primitive mantle values (McDonough and Sun, 1995), respectively.

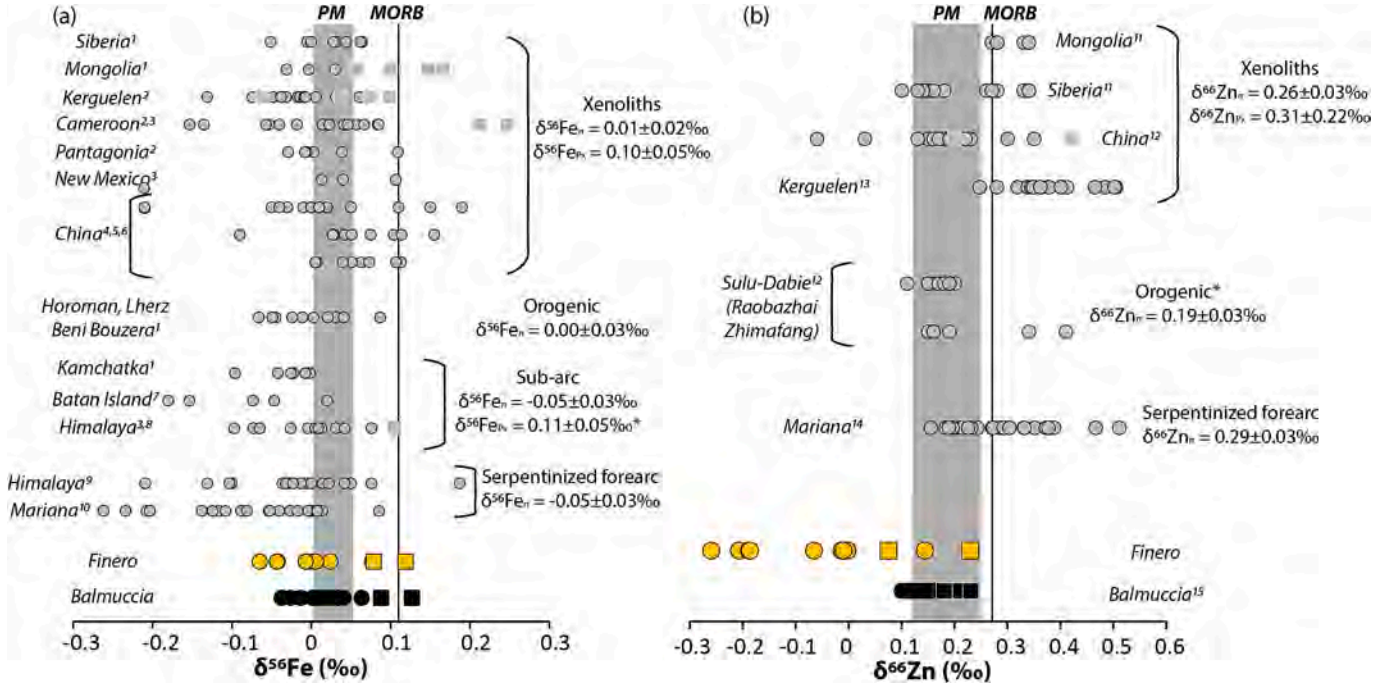

Fig. 5. Fe and Zn isotopic ranges of Balmuccia and Finero ultramafic rocks compared with mantle peridotite and pyroxenite worldwide. Primitive mantle values are from Craddock et al. (2013) and Sossi et al. (2018) for Fe and Zn isotopes, respectively. Data are form: 1, Weyer and Ionov (2007); 2, Poitrasson et al. (2013); 3, Williams et al. (2005); 4, Huang et al. (2011); 5, Zhao et al. (2012); 6, Zhao et al. (2015); 7, Turner et al. (2018); 8, Zhang et al. (2019); 9, Su et al. (2015); 10, Debret al. (2020); 11, Doucet et al. (2016); 12: Wang et al. (2017); 13: Beunon et al. (2020); 14: Debret et al., 2024; 15: Sossi et al. (2018).

has experienced melt extraction and its capacity to produce partial melts, is often expressed using CaO, Al_2O_3 and MgO contents. Fertile lherzolites display high CaO or Al_2O_3 and low MgO relative to refractory harzburgites and dunites (e.g., Bodinier and Godard, 2013). The studied samples display a negative covariation between CaO or Al_2O_3 and MgO contents with pyroxenites displaying the highest CaO or Al_2O_3 and lowest MgO contents and peridotites showing lower CaO or Al_2O_3 and MgO contents relative to the primitive mantle (Fig. 3). This reflects a decrease in modal clinopyroxene passing from pyroxenites to peridotites. One peridotite sample (BM-14) displays intermediate composition with abnormally high CaO (7.21 wt%) or Al_2O_3 (4.13 wt%) and low MgO (31.79 wt%) contents, reflecting lithological heterogeneities at sample scale (i.e., mixing with pyroxenite) during sample crushing. It must be noted that Finero peridotites record a large range of fertility, from lherzolite to dunite -like compositions. This variability contrasts with the forearc peridotites that commonly experienced very high degrees (>20 %) of melt extraction and display pyroxene poor harzburgite to dunite like compositions (e.g., Parkinson and Pearce, 1998).

The change in major element contents of peridotites during partial melting can be quantified through a non-modal batch melting model developed by Shaw (1970). Although this approach is not strictly applicable, because the partition coefficient must change as a function of melt fraction, it suffices to demonstrate the concept. Using the partitioning and modal melting reaction coefficients determined at 3 GPa by Walter (1998, 2003), this model is presented in Fig. 3 along with peridotite CaO, Al_2O_3 and MgO contents. Mineral modes, partition coefficients and modal melting reaction coefficients can be found in Supplementary Table 3. It should be noted that pressure has minimal effect on partitioning and modal melting reaction coefficients below 3 GPa (Walter, 1998). This melt modelling successfully fits the CaO, Al_2O_3 and MgO compositions of the peridotite dataset, suggesting that the observed major element geochemical diversity can be explained by different degrees of partial melting. However, as this lithological heterogeneity occurs at the metre-scale, partial melting is not likely to have occurred in-situ by adiabatic decompression in the mantle, as the peridotite massifs are km-sized.

As shown in Fig. 5, the isotopically heavy composition of MORB relative to primitive mantle (Teng et al., 2013; Sossi et al., 2016), indicates that melting processes are expected to decrease both the δ^{56}Fe and δ^{66}Zn values in peridotites, resulting in isotopically light peridotites that experienced extensive melt extraction (Doucet et al., 2016; Williams et al., 2004). Interestingly, negative covariations between either δ^{56}Fe and δ^{66}Zn and indices of peridotites fertility are observed in our samples (Fig. 6). However, previous attempts to model the behaviour of δ^{56}Fe and δ^{66}Zn during partial melting (e.g., Williams et al., 2004; Weyer and Ionov, 2007; Williams and Bizimis, 2014; Dauphas et al., 2017; Sossi and O'Neill, 2017; Sossi et al., 2018; Beunon et al., 2020) have shown that melting has only a limited effect on the isotopic composition of residual peridotite. For example, 30 % of partial melting will shift the δ^{56}Fe and δ^{66}Zn of less than 0.1 ‰ in the residual peridotite at pressures <3 GPa. It must be noted that Doucet et al. (2016) suggested a higher Zn isotope fractionation during high degree of partial melting, which was reconsidered as unrealistic by most recent studies (e.g., Sossi et al., 2018; Beunon et al., 2020). Furthermore, Fang et al. (2022) recently duplicated four fertile lherzolites from Doucet et al. (2016) and concluded that previously highly fractionated δ^{66}Zn values for mantle peridotites were due to analytical problems.

Here we used the non-modal batch melting model developed by Sossi and O'Neill (2017) for isotope partitioning to model both δ^{56}Fe and δ^{66}Zn values for peridotites during partial melting at 1300 °C. These models, which are presented in Fig. 6, employ *melt-mineral* fractionation factors from Sossi and O'Neill (2017) and Sossi et al. (2018) for Fe and Zn, respectively (Supplementary Table 3). Consistent with previous studies (e.g., Nebel et al., 2015; Dauphas et al., 2017; Sossi et al., 2018), the isotopic composition of peridotite is minimally affected by melting processes (up to 0.03 ‰ lighter at $f = 0.3$ for Fe and Zn) because most of

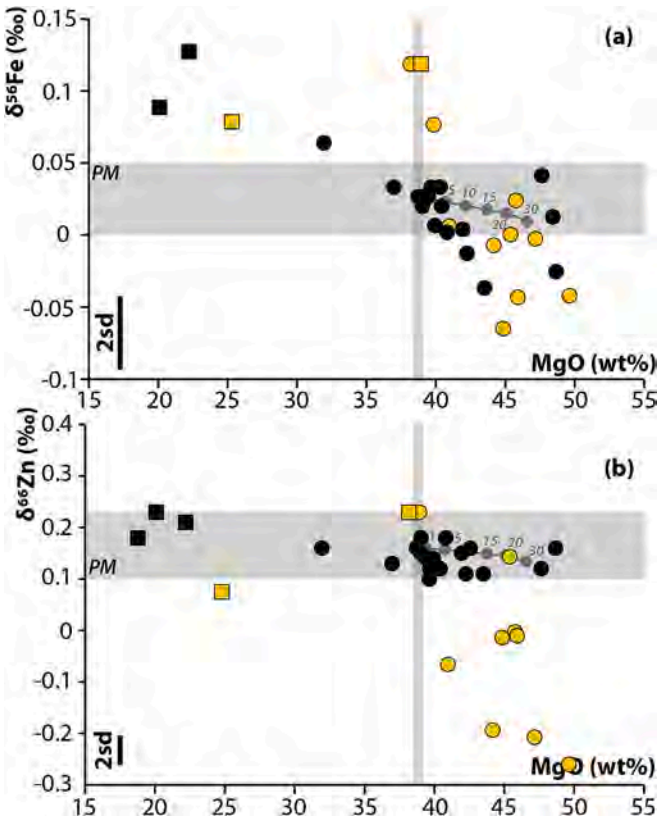

Fig. 6. Plots of (a) δ^{56}Fe and (b) δ^{66}Zn versus MgO contents. Non-Modal batch melting model are shown in grey line, see main text and Supplementary Table 3 for more details about the model.

the Fe and Zn remains in the source, limiting the amount of fractionation that can develop in the residue by the lever rule. The models provide an adequate description of the observed Zn isotope composition of Balmuccia peridotites, though some samples tend to display lower δ^{56}Fe values relative to that predicted by non-modal batch melting models. A similar observation was reported by Dauphas et al. (2017) who suggested that the used isotope fractionation coefficients between melt and minerals are not well enough documented to predict the full extent of Fe isotope fractionation during partial melting.

On the other hand, the δ^{56}Fe variations of Finero peridotites overlap with those of the Balmuccia samples. However, their Zn elemental and isotopic compositions show values that are too low (Figs. 5b & 6b) to be explained by non-modal batch melting. For a given MgO content, there is a consistent shift of up to 0.3 ‰ in δ^{66}Zn between peridotites from Finero and those from Balmuccia. While some variability is expected in mantle peridotites worldwide (Fig. 6), which might reflect some mantle heterogeneities at the global scale, Finero samples display isotopically light Zn compositions relative to mantle peridotites from other tectonic settings such as cratonic mantle and serpentinized forearc peridotites. This suggests that the isotope signatures of the Finero peridotites are incompatible with regional mantle heterogeneities with the most straightforward explanation being the influence of subduction-related component.

5.2. *High pressure metasomatism*

Metasomatism in a subduction setting can be related to C-O-S-H fluids and/or hydrous melts, which are generated in the wedge or in the slab. The Finero samples exhibit significant enrichment in the LREE relative to the HREE (La_N/Yb_N = 0.7–11.5), which is absent in unmetasomatized Balmuccia ultramafic rocks (Figs. 4 and 7). Such "spoon shape" fractionation is typically recorded by suprasubduction

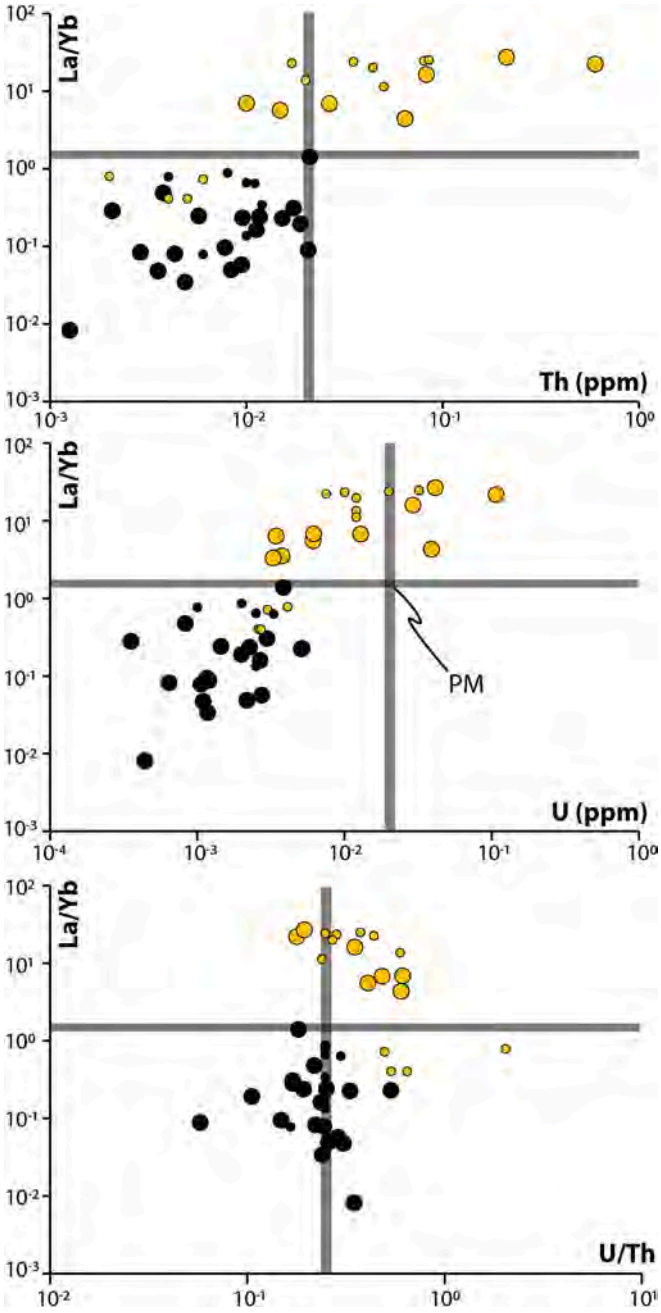

Fig. 7. Plots of La/Yb versus (a) Th (ppm), (b) U (ppm) concentrations and (c) U/Th ratios in Balmuccia and Finero peridotites. Litterature date are in small symbol (data from Hartmann and Wedepohl, 1993).

peridotites metasomatized by crust-derived fluid phases (e.g., Scambelluri et al., 2006; Malaspina et al., 2006, 2023). It is likely due to the high modal amount of clinopyroxene that partitions LREE with respect to the other mineral phases. These enrichments in LREE are also correlated with an increase of LILE concentrations (e.g., Cs, Rb) in the bulk rock (Fig. 4). The later are commonly interpreted as a contribution of slab derived fluids. Indeed, through prograde metamorphism, the concentration of LILE decreases in metasedimentary rock by progressive devolatilization (Bebout et al., 2007; Bebout et al., 1999). Similarly, slab-derived aqueous/supercritical liquids are expected to fractionate LREE elements relative to HREE. Hence the contribution of slab derived component in Finero peridotites can explain the observed enrichments in LREE and LILE. In agreement with this interpretation, the Finero geochemical patterns, characterized by a depletion in major elements, but enriched in K, Rb, Ba, Sr and LREE, were first attributed by Zanetti et al. (1999) to a slab-derived "carbonatite" melt component where pyroxenites are regions of high concentrations of such melt. Similarly, Selverstone and Sharp (2011) proposed that metasomatism by fluids released from a downgoing slab produced the $\delta^{37}Cl$ composition of Finero phlogopite-bearing peridotite, while amphibole-bearing peridotites require an additional melt component. To distinguish between metasomatism related to hydrous fluids or silicate melts at eclogite facies conditions it is instructive to examine the behaviour of a variety of trace elements, most notably U, Th and LREE among these phases (Kessel et al., 2005). In particular, at 900 °C, it is possible to discriminate fluids from melt or supercritical fluids based on excess of U over Th (U/Th $>>$ 1). Peridotite La/Yb ratios increase with U and Th concentrations, with Balmuccia samples having the lowest and Finero samples having the highest La/Yb ratios, U and Th concentrations (Fig. 7a-b). Lanthanum is relatively more mobile in fluids or melts than Yb, such that highly metasomatized samples should display the highest La/Yb ratios. Hence, these observations suggest a high degree of metasomatism in Finero relative to Balmuccia samples. However, Th is sparingly soluble in fluids (Kessel et al., 2005), making difficult to reconcile trace element enrichment in Finero peridotites with metasomatism by an aqueous fluid. Although U/Th ratios are relatively constant between the studied massifs (Fig. 6c), U/Th is negatively correlated with La/Yb ratios in Finero samples. This might suggest a slightly higher mobility of Th relative to U during metasomatic processes. In melts, the partitioning of Th is similar (U/Th ~ 1) at 900 °C to slightly higher (U/Th > 1) at 1000 °C to that of U (inferred peak temperature in Finero) while, at these conditions, an excess of Th over U is always expected in supercritical liquids (Kessel et al., 2005). Metasomatism by both melts and supercritical liquids can explain the composition of Finero peridotites. However, the occurrence of supercritical liquids in subduction systems requires pressure > 2.3 GPa for sedimentary systems, > 3.4 GPa for basaltic systems and > 4 GPa for ultramafic systems (Ni et al., 2017). Hence, a direct metasomatism by supercritical fluid phases is unlikely due the low-pressure conditions record of Finero massif.

5.3. *Deciphering the nature of Finero metasomatism using stable isotopes*

During subduction, numerical models (e.g., Syracuse et al., 2010) suggests that top slab temperatures might be high enough to cross the wet solidus for hydrated sediments and altered oceanic crust in most arcs. However, both HP-slab derived sediments ($\delta^{66}Zn = +0.40 \pm 0.13$ ‰; Debret et al., 2021) or eclogite crust ($\delta^{66}Zn = +0.22 \pm 0.13$ ‰; Inglis et al., 2017) display high $\delta^{66}Zn$ values relative to mantle peridotites. Also, on the whole, silicate melts preferentially complex heavy zinc isotopes relative to the residual peridotite as shown, for example, by the heavy zinc signature of MORB relative to mantle peridotites (Fig. 5b). The metasomatism of the mantle wedge by slab-derived melts will therefore result in the transfer of a heavy zinc component and therefore shift mantle wedge peridotites toward heavy values, which is not observed in Finero, therefore calling for other mechanisms.

Zinc isotope fractionation during slab devolatilization is intimately linked to Zn complexation in metamorphic fluids. It has recently been proposed that the transfer of isotopically heavy zinc from the slab to the mantle wedge occurs by oxidizing fluids carrying, for example, carbonate (e.g., Zn–CO_3; Debret et al., 2021) or sulfate (e.g., Zn–SO_4; Pons et al., 2016) ligands. More reduced fluids carrying, for example, Zn $(HS)_4^{2-}$ will have isotopically light Zn isotopic signatures (Debret et al., 2018). Theory also predicts that S-bearing fluids (either Fe-bearing sulfate- or sulfide-rich) will have isotopically light Fe isotope signatures (Fujii et al., 2014), compatible with that of the Finero peridotite (Fig. 5).

In order to explore any potential link between the Zn and Fe signatures of metasomatized samples and the transfer of a redox sensitive element (S or C), we investigated the fO_2 conditions recorded by mantle wedge peridotites. The fO_2 was calculated using the olivine-

orthopyroxene-spinel (OOS) equilibrium reaction:

$$6Fe_2SiO_4 + O_2 = 3Fe_2Si_2O_6 + 2Fe_3O_4 \quad (1)$$

Assessment of the oxygen fugacity requires treatment of the activity-composition relations of mineral solid solutions of the samples. For olivine and orthopyroxene, this is largely a function of Fe—Mg substitutions, which mix symmetrically and near-ideally (O'Neill et al., 2003; Wiser and Wood, 1991). The magnetite component in spinel is more complex; the experimental work by Wood (1990) shows that $Fe^{3+}/\Sigma Fe$ (aFe_3O_4) is a positive function of the Cr content as well as the $fO2$. If not accounted for, this leads to a systematic overestimation of fO_2 as a function of Cr content of spinel (e.g. Mattioli and Wood, 1988), which increases from lherzolite to dunite. A comparison of the expressions of O'neill and Wall (1987), Mattioli and Wood (1988) and Nell and Wood (1991), Wood (1990) showed that the Nell-Wood parameterization provided the most accurate fO_2, with a deviation of no more than 0.35 log units, and no systematic bias on Cr content. Therefore, the fO_2 estimates determined by the Nell and Wood (1991) calibration were used (Supplementary Table 4; see also Davis et al. (2017) for a recent assessment).

According to these calculations, Finero peridotites equilibrated at a fO_2 ranging between +0.2 and + 1 log units above the Fayalite-Magnetite-Quartz buffer (ΔFMQ). These variations are close to that reported in metasomatized supra-subduction garnet peridotite samples from Sulu belt (China) and Ulten Zone (Italian Central Alps), along with UHP garnet peridotites from Bardane (Western Gneiss Region, Norway) by Malaspina et al. (2009) and (Malaspina et al., 2010) based on Fe^{3+} contents of metamorphic garnet. Reported values range from −1.2 ± 1 (for the deepest samples of Bardane – 6 GPa) to +1.1 ± 0.4 (for the Sulu and Ulten peridotites – 5 GPa and 3 GPa, respectively) relative to FMQ buffer. They are also consistent with fO_2 calculated for spinel peridotite xenoliths from other subduction settings, typically ranging from −1 to +2 relative to FMQ buffer (Brandon and Draper, 1996; Cottrell et al., 2021; Parkinson and Arculus, 1999; Peslier et al., 2002). As already observed by Malaspina et al. (2009), the orogenic samples do not follow a trend of decreasing fO_2 with pressure, such as recorded by sub-cratonic xenoliths (Woodland and Koch, 2003). In contrast, OOS oxybarometry in Balmuccia peridotites record lower fO_2 (ΔFMQ = 0) than in the Finero peridotites, more in line with the oxygen fugacities recorded by mid-ocean ridge peridotites (ΔFMQ = 0 ± 0.4; Birner et al., 2018) or other massif peridotites (ΔFMQ ~0) (Davis et al., 2017; Woodland et al., 1992).

The more oxidised nature of the Finero peridotites is inconsistent with the circulation of reduced fluids with an isotopically light Zn isotope signature in the massif. However, it suggests a causal link between occurrence of metasomatic phases such as phlogopite, dolomite and amphibole therein and oxidation. These hydrous and carbonate rich phases require a metasomatism driven by fluids potentially equilibrated above the CCO ($C + O_2 = CO_2$) oxygen buffer, which, at 1.5 GPa defines an fO_2 within 0.2 log units of the FMQ buffer and becomes relatively more oxidizing as pressure increases (e.g., Frost and Wood, 1995). The stability of dolomite in these rocks is a further evidence for metasomatism at fO_2s above the FMQ buffer. Our fO_2 estimates show that this metasomatic event is such that the present equilibrium state of the Finero massif records ~ΔFMQ +1, at 900 °C and 1.2–1.6 GPa, hence being suggestive of chemical exchange at high fO_2 between mantle wedge peridotites and slab fluids. It must be noted that these high fO_2 conditions do not preclude the formation of Fe(II) species in fluids or rocks, as for example Fe(II)-rich meta-peridotites were reported at highly oxidizing conditions (i.e., FMQ + 3). This conclusion is also consistent with arc magma studies that predict, based on $Fe^{3+}/\sum Fe$ ratio measurements, a mantle wedge area equilibrated nearby ~ΔFMQ +1.5 ± 1 (Behrens and Gaillard, 2006; Carmichael, 1991; Gaborieau et al., 2020; Kelley and Cottrell, 2009). Although our fO_2 estimates in orogenic peridotites are suggestive of oxidation reactions associated with slab fluid transfer in subduction zone, Malaspina et al. (2009) showed that the addition of components such as K_2O, H_2O and CO_2, and therefore formation of phlogopite, amphibole and carbonates, can lead to variations in oxygen chemical potential (i.e., fO_2), unrelated to net whole-rock oxidation or reduction. The elevated fO_2 values recorded in the Finero samples are associated with either light $\delta^{56}Fe$ and $\delta^{66}Zn$ values relative to PM (Fig. 8), which suggests a concomitant oxidation and isotope fractionation of mantle wedge peridotites through metasomatic processes. In addition, the mobility of isotopically light Fe in slab fluids is inferred to result from the presence of Fe(II)-CO_3 or Fe(II)-SO_4 complexes equilibrated up to Hematite-Magnetite buffer (~ΔFMQ +3; Debret et al., 2016). Hence, association of light $\delta^{66}Zn$ and possibly $\delta^{56}Fe$ values with high fO_2 in refractory peridotites require an external oxidative agent. However, neither a direct transfer of aqueous slab fluids or silicate melts can simultaneously explain the trace element- and Fe—Zn isotopic signatures of the Finero peridotites.

Previous petrographic and geochemical studies have proposed that the Finero massif could record a multistage fluid evolution, with Finero phlogopite-bearing peridotite resulting from a carbon rich hydrous melt metasomatism that subsequently exsolves a carbon rich agent during its exhumation to the surface (Morishita et al., 2003). Evidence for a carbon rich metasomatism includes the occurrence of apatite and carbonate rich layers in Finero peridotites (Zanetti et al., 1999; Morishita et al., 2003). The formation of these layers was attributed to the crystallization of carbonatitic melts at upper mantle conditions. Similarly, carbon isotope ($\delta^{13}C$) investigations of Finero peridotites show enrichments in C relative to the deep mantle (Cannaò et al., 2022). Additional micro-Raman investigations by Cannaò et al. (2022) document the occurrence of graphite and carbonate bearing fluid inclusions, specifically in olivine and clinopyroxene, that are likely responsible for the high C concentrations reported in Finero peridotites.

Carbon rich fluid metasomatim in an open system is likely to produce high ratio of pyroxenes, as well as the crystallization of apatite, amphibole and/or phlogopite and the release of CO_2-rich fluids as the massif cross between 1.5 and 2 GPa the following reaction (e.g., Sapienza et al., 2009):

(1) enstatite + dolomite = forsterite + diopside + CO_2

The high abundance of pyroxene, phlogopite and amphibole in Finero peridotites (Fig. 2) and the presence of carbon rich fluid inclusions are consistent with such a reaction. Similarly, carbon rich fluid metasomatism is expected to increase Nb/Ta and Zr/Hf ratios in mantle peridotite (e.g., Chakhmouradian, 2006; Rudnick et al., 1993). In agreement with this, Finero peridotites display high Zr/Hf ratios (33–66) relative to Balmuccia peridotites (Zr/Hf = 12–37).

The complexes Zn-CO_3 in fluid form are among the isotopically heaviest complexes that could form on Earth (Fujii et al., 2014). Hence, the formation of metasomatic minerals (e.g., phlogopite, pyroxenes or carbonates) through the dissociation of a carbonate rich agent (e.g., eq. (1)) will necessarily favour the formation of an isotopically light Zn peridotite and the release of an isotopically heavy Zn fluid (or melt). This is supported by a negative correlation between Zr/Hf ratios and $\delta^{66}Zn$ values in Finero peridotites (on a restricted amount of analyses, see Supplementary Fig. 2). To further test such a hypothesis, we attempted to model the evolution of $\delta^{66}Zn$ in peridotites through the dissociation of a carbonate rich fluid. The behaviour of Zn in fluid was approximated to that of Zn-CO_3 complexes in aqueous fluids using the ab initio calculations of Fujii et al. (2014) as, to our knowledge, the behaviour of Zn-CO_3 complexes in melts remains unknown. The elemental and isotopic behaviour of Zn in peridotite was modelled using the available ab initio calculations of Ducher et al. (2016) for smithsonite ($ZnCO_3$), hydrozincite ($Zn_5(CO_3)_2(OH)_6$) and hemimorphite ($Zn_4Si_2O_7H_2O$)) assuming to represent Zn behaviour in carbonates and silicate, respectively. The calculated fractionation factors between carbonate rich fluids and minerals ($\alpha_{CO2\text{-}minerals}$) are displayed in Fig. 9a. At 900 °C, the 1000 x ln ($\alpha_{CO2\text{-}minerals}$) ranges between 0.1 and 0.2, with

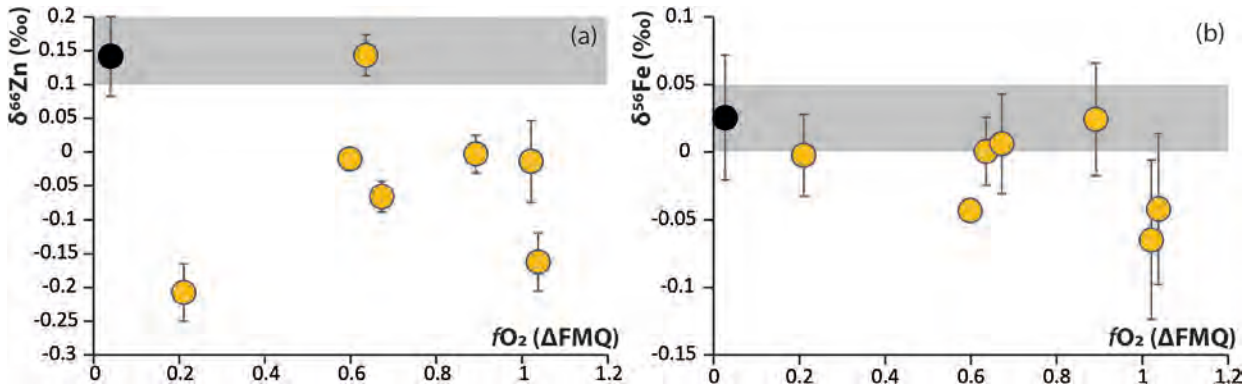

Fig. 8. (a) Zn and (b) Fe isotope ratios versus oxygen fugacity estimates relative to FMQ ($\Delta = \log fO_2^{\ sample} - \log fO_2^{FMQ}$). The grey area correspond to primitive mantle values.

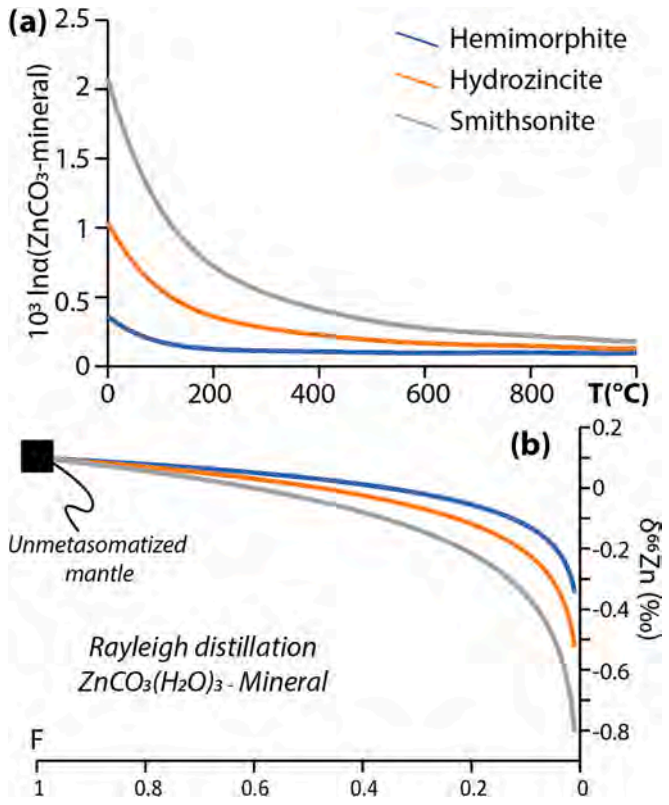

Fig. 9. (a) Calculated Zn fractionation factors between $ZnCO_3$ in fluids and metasomatic minerals like phlogopite or amphibole, approximated to hemimorphite ($Zn_4Si_2O_7(OH)_2H_2O$), and solid carbonates such as hydrozincite ($Zn_5(CO_3)_2(OH)_6$) and smithsonite ($ZnCO_3$) based on ab initio calculations of Fujii et al. (2014) and Ducher et al. (2016). (b) Rayleigh distillation modelling the dissociation of a carbonate component during peridotite metasomatism.

$\alpha_{CO2\text{-}smithsonite} > \alpha_{CO2\text{-}hydrozincite} > \alpha_{CO2\text{-}hemimorphite}$. Hence, the formation of either carbonate or hydrous silicate during carbonate rich fluid metasomatism in an open system is expected to decrease the $\delta^{66}Zn$ of peridotite. The $\delta^{66}Zn$ evolution of peridotite was then modelled using a simple Rayleigh distillation model, according to the following equation:

$$(2)\ \delta_f - \delta_i = 1000\ (F^{(\alpha-1)}-1)$$

where δ_f and δ_i are the initial and final isotopic value of the peridotite, F is the fraction of Zn that remains in the rock, ranging from 1 (unreacted) to 0 (all the Zn is lost in the fluid phase), and α is the fractionation factor ($\alpha_{CO2\text{-}minerals}$) at 900 °C, i.e., metamorphic peak P-T conditions of the Finero massif. The initial composition of the peridotite was set to a mantle like value (+0.1 ‰; Sossi et al., 2018). Results of this model are displayed in Fig. 9b. The $\delta^{66}Zn$ values of Finero peridotites ranging from 0 to −0.26 ‰ can be modelled through the extraction of about 40 to 80 ‰ of the zinc. It must be noted that exchanges of Zn between peridotite and carbon rich fluids or melts in an open system has the potential to significantly affect the isotopic signature of the host peridotite as for example carbonatite produce by immiscibility processes display high Zn concentrations (up to 86 ppm, Martin et al., 2013) relative to mantle peridotites. However, such a process will have negligible impact on the $\delta^{56}Fe$ of mantle peridotites as the solubility of Fe in either carbon bearing fluid or carbonatite melt is low (< 1 wt%; (Berkesi et al., 2020; Scambelluri et al., 2015) relative to the Fe content of mantle peridotites.

5.4. Conclusions and perspectives

Investigations of Balmuccia peridotites show that their geochemical signatures can be achieved through simple non-modal batch melting model. In contrast, both trace element concentrations and Zn stable isotopes of phlogopite- and amphibole-bearing peridotites in the Finero massif point toward the addition of a metasomatizing agent. Based on trace elements patterns of Finero peridotites, the parent metasomatizing agent was likely a melt carrying an excess of Th and LREE over U and HREE, respectively. The presence of supercritical fluids was ruled out due to the low-pressure record of the massif. Correlations between LREE/HREE ratios and LILE concentrations in Finero peridotites suggest an influence of a slab derived melt. This is consistent with previous trace element and radiogenic isotopic interpretations inferring the involvement of sedimentary component in the metasomatic overprint of the Finero Peridotite massif (Hartmann and Hans Wedepohl, 1993; Zanetti et al., 1999). Strangely, the light Zn isotope signature of Finero peridotites is incompatible with a direct metasomatism by slab derived melts, the latter being necessarily heavy relative to mantle peridotites. Such a contrasting signature between trace elements and Zn isotopes can be reconciled through a metasomatism by carbon rich fluids (or melts) in an open system. This process is likely to produce phlogopite or amphibole bearing peridotites with an abnormally light Zn isotope signature and the release of isotopically heavy CO_2-rich fluids.

CRediT authorship contribution statement

B. Debret: Writing – original draft, Visualization, Validation, Supervision, Resources, Project administration, Methodology, Investigation, Funding acquisition, Formal analysis, Data curation, Conceptualization. **P.A. Sossi:** Writing – original draft, Methodology, Investigation, Data curation, Conceptualization. **N. Malaspina:** Writing – original draft, Conceptualization. **A. Gautier:** Writing – original draft,

Formal analysis, Data curation. **N. Mattielli:** Writing – original draft, Funding acquisition, Conceptualization. **H. O'Neill:** Writing – original draft, Data curation. **J. Villalobos-Orchard:** Writing – original draft, Formal analysis, Data curation. **F. Moynier:** Writing – original draft, Funding acquisition.

Declaration of competing interest

The authors declare that they have no known competing financial interests or personal relationships that could have appeared to influence the work reported in this paper.

Acknowledgments

The authors thank H. Beunon, K. Koga and C. Nicollet for their assistance during the Finero 2018 field trip, J. Devidal for its help during microprobe analyses, P. Burkel, Tutu and D. Rigoussen for their precious help during geochemical analyses. We thank Zuxing Chen and Tomo Moroshita for critical comments on earlier version of this article and careful editorial handling by Sonja Aulbach. This study was initiated by an Institut de Physique du Globe de Paris Visiting position attributed to N. Malaspina. This work was supported by the IPGP analytical platform PARI, Region Ile-de-France SESAME Grants no. 12015908, and DIM ACAV +, the ERC grant agreement No. 101001282 (METAL) (F.M.), the Agence Nationale de la Recherche (ANR) CARBioNic "ANR-22-CE49-0001-01" (B.D.) and the Fond National de la Recherche Scientifique de Belgique (FNRS).

Appendix A. Supplementary data

Supplementary data to this article can be found online at https://doi.org/10.1016/j.chemgeo.2025.122649.

Data availability

Data are available in supplementary material.

References

Archer, C., Andersen, M.B., Cloquet, C., Conway, T.M., Dong, S., Ellwood, M., Moore, R., Nelson, J., Rehkämper, M., Rouxel, O., Samanta, M., Shin, K.C., Sohrin, Y., Takano, S., Wasylenki, L., 2017. Inter-calibration of a proposed new primary reference standard AA-ETH Zn for zinc isotopic analysis. J. Anal. At. Spectrom 32, 415–419. https://doi.org/10.1039/c6ja00282j.

Bebout, G.E., Ryan, J.G., Leeman, W.P., Bebout, A.E., 1999. Fractionation of trace elements by subduction-zone metamorphism — effect of convergent-margin thermal evolution. Earth Planet. Sci. Lett. 171, 63–81. https://doi.org/10.1016/S0012-821X(99)00135-1.

Bebout, G.E., Bebout, A.E., Graham, C.M., 2007. Cycling of B, Li, and LILE (K, Cs, Rb, Ba, Sr) into subduction zones: SIMS evidence from micas in high-P/T metasedimentary rocks. Chem. Geol. 239, 284–304. https://doi.org/10.1016/j.chemgeo.2006.10.016.

Behrens, H., Gaillard, F., 2006. Geochemical Aspects of Melts: Volatiles and Redox Behavior. Elements 2, 275–280. https://doi.org/10.2113/gselements.2.5.275.

Berkesi, M., Bali, E., Bodnar, R.J., Szabó, Á., Guzmics, T., 2020. Carbonatite and highly peralkaline nephelinite melts from Oldoinyo Lengai Volcano, Tanzania: the role of natrite-normative fluid degassing. Gondw. Res. 85, 76–83.

Beunon, H., Mattielli, N., Doucet, L.S., Moine, B., Debret, B., 2020. Mantle heterogeneity through Zn systematics in oceanic basalts : evidence for a deep carbon cycling. Earth-Science Rev. 205, 103174.

Birner, S.K., Cottrell, E., Warren, J.M., Kelley, K.A., Davis, F.A., 2018. Peridotites and basalts reveal broad congruence between two independent records of mantle fO2 despite local redox heterogeneity. Earth Planet. Sci. Lett. 494, 172–189. https://doi.org/10.1016/j.epsl.2018.04.035.

Bodinier, J.L., Godard, M., 2013. Orogenic, ophiolitic, and abyssal peridotites, 3rd ed. In: Treatise on Geochemistry, Second edition. Elsevier Ltd. https://doi.org/10.1016/B978-0-08-095975-7.00204-7

Brandon, A.D., Draper, D.S., 1996. Constraints on the origin of the oxidation state of mantle overlying subduction zones: An example from Simcoe, Washington, USA. Geochim. Cosmochim. Acta 60, 1739–1749. https://doi.org/10.1016/0016-7037(96)00056-7.

Cannaò, E., Tiepolo, M., Fumagalli, P., Grieco, G., Agostini, S., 2022. Metasomatism in the Finero Phlogopite Peridotite: New insights from C and N concentrations and δ13C - δ11B signatures. Chem. Geol. 614, 121181. https://doi.org/10.1016/j.chemgeo.2022.121181.

Carignan, J., Hild, P., Mevelle, G., Morel, J., Yeghicheyan, D., 2001. Routine analyses of trace elements in geological samples using flow injection and low pressure on-line liquid chromatography coupled to ICP-MS: a study of geochemical reference materials BR, DR-N, UB-N, AN-G and GH. Geostand. Newslett. 25, 187–198. https://doi.org/10.1111/j.1751-908x.2001.tb00595.x.

Carmichael, I.S.E., 1991. The redox states of basic and silicic magmas: a reflection of their source regions? Contrib. Mineral. Petrol. 106, 129–141. https://doi.org/10.1007/BF00306429.

Chakhmouradian, A.R., 2006. High-field-strength elements in carbonatitic rocks: geochemistry, crystal chemistry and significance for constraining the sources of carbonatites. Chem. Geol. 235, 138–160.

Chen, Y., Su, B., Chu, Z., 2017. Modification of an ancient subcontinental lithospheric mantle by continental subduction: Insight from the Maowu garnet peridotites in the Dabie UHP belt, eastern China. Lithos 278–281, 54–71. https://doi.org/10.1016/j.lithos.2017.01.025.

Chen, Z., Chen, J., Tamehe, L.S., Zhang, Y., Zeng, Z., Zhang, T., Shuai, W., Yin, X., 2023. Light Fe isotopes in arc magmas from cold subduction zones: Implications for serpentinite-derived fluids oxidized the sub-arc mantle. Geochim. Cosmochim. Acta 342, 1–14. https://doi.org/10.1016/j.gca.2022.12.005.

Chou, I., Eugster, H., 1977. Solubility of magnetite in supercritical chloride solutions. Am. J. Sci. 277, 1296–1314.

Class, C., Miller, D.M., Goldstein, S.L., Langmuir, C.H., 2000. Distinguishing melt and fluid subduction components in Umnak Volcanics, Aleutian Arc. Geochemistry. Geophys. Geosystems 1, 1–28. https://doi.org/10.1029/1999GC000010.

Cottrell, E., Birner, S.K., Brounce, M., Davis, F.A., Waters, L.E., Kelley, K.A., 2021. Oxygen fugacity across tectonic settings. In: Magma Redox Geochemistry. American Geophysical Union (AGU), pp. 33–61. https://doi.org/10.1002/9781119473206.ch3.

Craddock, P.R., Warren, J.M., Dauphas, N., 2013. Abyssal peridotites reveal the near-chondritic Fe isotopic composition of the Earth. Earth Planet. Sci. Lett. 365, 63–76. https://doi.org/10.1016/j.epsl.2013.01.011.

Dauphas, N., Craddock, P.R., Asimow, P.D., Bennett, V.C., Nutman, A.P., Ohnenstetter, D., 2009. Iron isotopes may reveal the redox conditions of mantle melting from Archean to present. Earth Planet. Sci. Lett. https://doi.org/10.1016/j.epsl.2009.09.029.

Dauphas, N., John, S.G., Rouxel, O., 2017. Iron isotope systematics. Non-Traditional Stable Isot. 82, 415–510. https://doi.org/10.2138/rmg.2017.82.11.

Davis, F.A., Cottrell, E., Birner, S.K., Warren, J.M., Lopez, O.G., 2017. Revisiting the electron microprobe method of spinel-olivine-orthopyroxene oxybarometry applied to spinel peridotites. Am. Mineral. 102, 421–435. https://doi.org/10.2138/am-2017-5823.

Debret, B., Millet, M.-A., Pons, M.-L., Bouilhol, P., Inglis, E., Williams, H., 2016. Isotopic evidence for iron mobility during subduction. Geology 44, 215–218. https://doi.org/10.1130/G37565.1.

Debret, B., Reekie, C.D.J., Mattielli, N., Beunon, H., Ménez, B., Savov, I.P., Williams, H. M., 2020. Redox transfer at subduction zones : insights from Fe isotopes in the Mariana forearc. Geochemical Perspect. Lett. 12, 46–51. https://doi.org/10.7185/geochemlet.2003.

Debret, B., Beunon, H., Mattielli, N., Andreani, M., Ribeiro da Costa, I., Escartin, J., 2018. Ore component mobility, transport and mineralization at mid-oceanic ridges: A stable isotopes (Zn, Cu and Fe) study of the Rainbow massif (Mid-Atlantic Ridge 36°14′N). Earth Planet. Sci. Lett. 503, 170–180. https://doi.org/10.1016/j.epsl.2018.09.009.

Debret, B., Garrido, C.J., Pons, M.L., Bouilhol, P., Inglis, E., López Sánchez-Vizcaíno, V., Williams, H., 2021. Iron and zinc stable isotope evidence for open-system high-pressure dehydration of antigorite serpentinite in subduction zones. Geochim. Cosmochim. Acta 296, 210–225. https://doi.org/10.1016/j.gca.2020.12.001.

Debret, B., Andreani, M., Godard, M., 2024. A review of abyssal serpentinite geochemistry and geodynamics. Earth-Science Rev. 258, 104910. https://doi.org/10.1016/j.earscirev.2024.104910.

Doucet, L.S., Mattielli, N., Ionov, D.A., Debouge, W., Golovin, A.V., 2016. Zn isotopic heterogeneity in the mantle: a melting control? Earth Planet. Sci. Lett. 451, 232–240. https://doi.org/10.1016/j.epsl.2016.06.040.

Ducher, M., Blanchard, M., Balan, E., 2016. Equilibrium zinc isotope fractionation in Zn-bearing minerals from first-principles calculations. Chem. Geol. 443, 87–96. https://doi.org/10.1016/j.chemgeo.2016.09.016.

Duncan, M.S., Dasgupta, R., 2017. Rise of Earth's atmospheric oxygen controlled by efficient subduction of organic carbon. Nat. Geosci. 10, 387–392. https://doi.org/10.1038/ngeo2939.

Eggins, S.M., Woodhead, J.D., Kinsley, L.P.J., Mortimer, G.E., Sylvester, P., McCulloch, M.T., Hergt, J.M., Handler, M.R., 1997. A simple method for the precise determination of ≥ 40 trace elements in geological samples by ICPMS using enriched isotope internal standardisation. Chem. Geol. 134, 311–326. https://doi.org/10.1016/S0009-2541(96)00100-3.

Eguchi, J., Seales, J., Dasgupta, R., 2020. Deep cycling and enhanced degassing of carbon. Nat. Geosci. 13. https://doi.org/10.1038/s41561-019-0492-6.

Elliott, T., 2004. Tracers of the slab. Geophys. Monogr. Ser. 138, 23–45. https://doi.org/10.1029/138GM03.

Elliott, T., Plank, T., Zindler, A., White, W., Bourdon, B., 1997. Element transport from slab to volcanic front at the Mariana arc. J. Geophys. Res. Solid Earth 102, 14,991–15,018.

Fang, S. Bin, Huang, J., Zhang, X.C., Ionov, D.A., Zhao, Z.F., Huang, F., 2022. Zinc isotope fractionation in mantle rocks and minerals, and a revised δ66Zn value for the Bulk Silicate Earth. Geochim. Cosmochim. Acta 338, 79–92. https://doi.org/10.1016/j.gca.2022.10.017.

Foden, J., Sossi, P.A., Nebel, O., 2018. Controls on the iron isotopic composition of global arc magmas. Earth Planet. Sci. Lett. https://doi.org/10.1016/j.epsl.2018.04.039.
Förster, B., Aulbach, S., Bebout, G.E., Bianchini, G., Natali, C., Braga, R., 2024. Iron-sulfur-carbon redox interactions in the continental subduction factory and their effect on volatile element storage in the mantle wedge. Earth Planet. Sci. Lett. 648, 119074.
Fountain, D., 1976. The Ivrea-Verbano and Strona-Ceneri zones, northern Italy: a cross-section of the continental crust – New evidence from seismic velocities of rock samples. Tectonophysics 33, 145–165.
Frost, D.J., Wood, B.J., 1995. Experimental measurements of the graphite C- O equilibrium and CO 2 fugacities at high temperature and pressure. Contrib. to Mineral. Petrol. 121, 303–308.
Fujii, T., Moynier, F., Blichert-Toft, J., Albarède, F., 2014. Density functional theory estimation of isotope fractionation of Fe, Ni, Cu, and Zn among species relevant to geochemical and biological environments. Geochim. Cosmochim. Acta 140, 553–576. https://doi.org/10.1016/j.gca.2014.05.051.
Gaborieau, M., Laubier, M., Bolfan-Casanova, N., McCammon, C.A., Vantelon, D., Chumakov, A.I., Schiavi, F., Neuville, D.R., Venugopal, S., 2020. Determination of Fe3+/ΣFe of olivine-hosted melt inclusions using Mössbauer and XANES spectroscopy. Chem. Geol. 547. https://doi.org/10.1016/j.chemgeo.2020.119646.
Gerrits, A.R., Inglis, E.C., Dragovic, B., Starr, P.G., Baxter, E.F., Burton, K.W., 2019. Release of oxidizing fluids in subduction zones recorded by iron isotope zonation in garnet. Nat. Geosci. 12, 1029–1033. https://doi.org/10.1038/s41561-019-0471-y.
Giovanardi, T., Mazzucchelli, M., Zanetti, A., Langone, A., Tiepolo, M., Cipriani, A., 2014. Occurrence of phlogopite in the Finero Mafic layered complex. Cent. Eur. J. Geosci. 6, 588–613. https://doi.org/10.2478/s13533-012-0186-8.
Hartmann, G., Hans Wedepohl, K., 1993. The composition of peridotite tectonites from the Ivrea complex, northern Italy: Residues from melt extraction. Geochim. Cosmochim. Acta 57, 1761–1782. https://doi.org/10.1016/0016-7037(93)90112-A.
Hawkesworth, C.J., Gallagher, K., Hergt, J.M., McDermott, F., 1993. Mantle and slab contributions in ARC magmas. Annu. Rev. Earth Planet. Sci. 21, 175–204.
Herzberg, C., 2004. Geodynamic information in peridotite petrology. J. Petrol. 45, 2507–2530. https://doi.org/10.1093/petrology/egh039.
Huang, F., Zhang, Z., Lundstrom, C.C., Zhi, X., 2011. Iron and magnesium isotopic compositions of peridotite xenoliths from Eastern China. Geochim. Cosmochim. Acta 75, 3318–3334.
Inglis, E.C., Debret, B., Burton, K.W., Millet, M.-A., Pons, M.-L., Dale, C.W., Bouilhol, P., Cooper, M., Nowell, G.M., McCoy-West, A.J., Williams, H.M., 2017. The behavior of iron and zinc stable isotopes accompanying the subduction of mafic oceanic crust: a case study from Western Alpine ophiolites. Geochemistry, Geophys. Geosystems 18. https://doi.org/10.1002/2016GC006735.
Johnson, M.C., Plank, T., 2000. Dehydration and melting experiments constrain the fate of subducted sediments. Geochemistry, Geophys. Geosystems 1. https://doi.org/10.1029/1999GC000014.
Kelley, K.A., Cottrell, E., 2009. Water and the oxidation state of subduction zone magmas. Science 325, 605–607. https://doi.org/10.1126/science.1174156.
Kessel, R., Schmidt, M.W., Ulmer, P., Pettke, T., 2005. Trace element signature of subduction-zone fluids, melts and supercritical liquids at 120-180 km depth. Nature 437, 724–727. https://doi.org/10.1038/nature03971.
Li, X.-L., Chen, Y.-X., Zhou, K., Xiong, J.-W., Demény, A., Schertl, H.-P., Huang, F., 2024. Iron mobility in subduction zone fluids at forearc depths and implications for mantle redox heterogeneity. Chem. Geol. 644, 121879.
Liu, S.A., Wang, Z.Z., Li, S.G., Huang, J., Yang, W., 2016. Zinc isotope evidence for a large-scale carbonated mantle beneath eastern China. Earth Planet. Sci. Lett. 444, 169–178. https://doi.org/10.1016/j.epsl.2016.03.051.
Lu, M., Hofmann, A.W., Mazzucchelli, M., Rivalenti, G., 1997. The mafic-ultramafic complex near Finero (IVZ), I. Chemistry of MORB-like magmas. Chem. Geol. 140, 207–222.
Malaspina, N., Hermann, J., Scambelluri, M., Compagnoni, R., 2006. Multistage metasomatism in ultrahigh-pressure mafic rocks from the North Dabie complex (China). Lithos 90, 19–42. https://doi.org/10.1016/j.lithos.2006.01.002.
Malaspina, N., Poli, S., Fumagalli, P., 2009. The oxidation state of metasomatized mantle wedge: Insights from C-O-H-bearing garnet peridotite. J. Petrol. 50, 1533–1552. https://doi.org/10.1093/petrology/egp040.
Malaspina, N., Scambelluri, M., Poli, S., Van Roermund, H.L.M., Langenhorst, F., 2010. The oxidation state of mantle wedge majoritic garnet websterites metasomatised by C-bearing subduction fluids. Earth Planet. Sci. Lett. 298, 417–426. https://doi.org/10.1016/j.epsl.2010.08.022.
Malaspina, N., Borghini, G., Zanchetta, S., Pellegrino, L., Corti, M., Tumiati, S., 2023. ▪ Geochemical evolution of melt / peridotite interaction at high pressure in subduction zones. Geochemical Perspect. Lett. 24, 48–52. https://doi.org/10.7185/geochemlet.2305.
Maréchal, C.N., Télouk, P., Albarède, F., 1999. Precise analysis of copper and zinc isotopic compositions by plasma-source mass spectrometry. Chem. Geol. 156, 251–273. https://doi.org/10.1016/S0009-2541(98)00191-0.
Marschall, H.R., Schumacher, J.C., 2012. Arc magmas sourced from mélange diapirs in subduction zones. Nat. Geosci. 5, 862–867. https://doi.org/10.1038/ngeo1634.
Martin, L.H.J., Schmidt, M.W., Mattsson, H.B., Guenther, D., 2013. Element partitioning between immiscible carbonatite and silicate melts for dry and H2O-bearing systems at 1–3 GPa. J. Petrol. 54, 2301–2338.
Matsumoto, T., Morishita, T., Matsuda, J.I., Fujioka, T., Takebe, M., Yamamoto, K., Arai, S., 2005. Noble gases in the Finero phlogopite-peridotites, western Italian Alps. Earth Planet. Sci. Lett. 238, 130–145. https://doi.org/10.1016/j.epsl.2005.07.005.
Mattioli, G.S., Wood, B.J., 1988. Magnetite activities across the MgAl2O4-Fe3O4 spinel join, with application to thermobarometric estimates of upper mantle oxygen fugacity. Contrib. Mineral. Petrol. 98, 148–162. https://doi.org/10.1007/BF00402108.
Mazzucchelli, M., Rivalenti, G., Brunelli, D., Zanetti, A., Boari, E., 2009. Formation of highly refractory dunite by focused percolation of pyroxenite-derived melt in the Balmuccia peridotite massif (Italy). J. Petrol. 50, 1205–1233.
McDonough, W.F., Sun, S.-S., 1995. The composition of the Earth. Chem. Geol. 120, 223–253.
Mehnert, K.R., 1975. The Ivrea Zone. A model of the deep crust. Neues Jahrb. für Mineral. Abhandlungen 125, 156–199.
Miller, D.M., Goldstein, S.L., Langmuir, C.H., 1994. Cerium/lead and lead isotope ratios in arc magmas and the enrichment of lead in the continents. Nature 368, 514–520. https://doi.org/10.1038/368514a0.
Morishita, T., Arai, S., Tamura, A., 2003. Petrology of an apatite-rich layer in the Finero phlogopite–peridotite, Italian Western Alps; implications for evolution of a metasomatising agent. Lithos 69, 37–49.
Morishita, T., Hattori, K.H., Terada, K., Matsumoto, T., Yamamoto, K., Takebe, M., Ishida, Y., Tamura, A., Arai, S., 2008. Geochemistry of apatite-rich layers in the Finero phlogopite–peridotite massif (Italian Western Alps) and ion microprobe dating of apatite. Chem. Geol. 251, 99–111.
Morris, J., Leeman, W.P., Tera, F., 1990. The subducted component in island arc lavas: constraints from be isotopes and B-Be systematics. Nature 344, 31–36.
Moynier, F., Vance, D., Fujii, T., Savage, P., 2017. The isotope geochemistry of zinc and copper. Non-Traditional Stable Isot. 82, 543–600. https://doi.org/10.2138/rmg.2017.82.13.
Nebel, O., Sossi, P.A., Bénard, A., Wille, M., Vroon, P.Z., Arculus, R.J., 2015. Redox-variability and controls in subduction zones from an iron-isotope perspective. Earth Planet. Sci. Lett. 432, 142–151. https://doi.org/10.1016/j.epsl.2015.09.036.
Nell, J., Wood, B.J., 1991. High-temperature electrical measurements and thermodynamic properties of Fe3O4-FeCr2O4-MgCr2O4-FeAl2O4 spinels. Am. Mineral. 76, 405–426.
Ni, H., Zhang, L., Xiong, X., Mao, Z., Wang, J., 2017. Supercritical fluids at subduction zones: evidence, formation condition, and physicochemical properties. Earth-Science Rev. 167, 62–71.
Nimis, P., Morten, L., 2000. P-T evolution of “crustal” garnet peridotites and included pyroxenites from Nonsberg area (upper Austroalpine), NE Italy: from the wedge to the slab. J. Geodyn. 30, 93–115. https://doi.org/10.1016/S0264-3707(99)00029-0.
O’neill, H.S.C., Wall, V.J., 1987. The Olivine—Orthopyroxene—Spinel Oxygen Geobarometer, the Nickel Precipitation Curve, and the Oxygen Fugacity of the Earth’s Upper Mantle. J. Petrol. 28, 1169–1191. https://doi.org/10.1093/petrology/28.6.1169.
O’Neill, H.S.C., Pownceby, M.I., McCammon, C.A., 2003. The magnesiowüstite: Iron equilibrium and its implications for the activity-composition relations of (Mg,Fe)2SiO4 olivine solid solutions. Contrib. Mineral. Petrol. 146, 308–325. https://doi.org/10.1007/s00410-003-0496-4.
Parkinson, I.J., Arculus, R.J., 1999. The redox state of subduction zones: Insights from arc-peridotites. Chem. Geol. 160, 409–423. https://doi.org/10.1016/S0009-2541(99)00110-2.
Parkinson, I.J., Pearce, J.A., 1998. Peridotites from the Izu-Bonin-Mariana forearc (ODP Leg 125): evidence for mantle melting and melt-mantle interaction in a supra-subduction zone setting. J. Petrol. 39, 1577–1618. https://doi.org/10.1093/petroj/39.9.1577.
Pearce, J.A., 1982. Trace element characteristics of lavas from destructive plate boundaries. In: Thorpe, R.S. (Ed.), Orogenic Andesites and Related Rocks, pp. 528–542.
Pellegrino, L., Malaspina, N., Zanchetta, S., Langone, A., Tumiati, S., 2020. High pressure melting of eclogites and metasomatism of garnet peridotites from Monte Duria Area (Central Alps, N Italy): a proxy for melt-rock reaction during subduction. Lithos 358–359, 105391. https://doi.org/10.1016/j.lithos.2020.105391.
Peslier, A.H., Luhr, J.F., Post, J., 2002. Low water contents in pyroxenes from spinel-peridotites of the oxidized, sub-arc mantle wedge. Earth Planet. Sci. Lett. 201, 69–86. https://doi.org/10.1016/S0012-821X(02)00663-5.
Plank, Terry, Langmuir, Charles H., 1993. Tracing trace elements from sediment input to volcanic output at subduction zones. Nature 362, 461–464.
Poitrasson, F., Delpech, G., Gregoire, M., 2013. On the iron isotope heterogeneity of lithospheric mantle xenoliths : implications for mantle metasomatism, the origin of basalts and the iron isotope composition of the Earth. Contrib. to Mineral. Petrol. 165, 1243–1258. https://doi.org/10.1007/s00410-013-0856-7.
Polyakov, V.B., Mineev, S.D., 2000. The use of Mossbauer spectroscopy in stable isotope geochemistry. Geochim. Cosmochim. Acta 64, 849–865. https://doi.org/10.1016/S0016-7037(99)00329-4.
Pons, M.-L., Debret, B., Bouilhol, P., Delacour, A., Williams, H., 2016. Zinc isotope evidence for sulfate-rich fluid transfer across subduction zones. Nat. Commun. 7, 13794. https://doi.org/10.1038/ncomms13794.
Quick, J.E., Sinigoi, S., Mayer, A., 1995. Emplacement of mantle peridotite in the lower continental crust, Ivrea-Verbano Zone, Northwest Italy. Geology 23, 739–742. https://doi.org/10.1130/0091-7613(1995)023<0739:EOMPIT>2.3.CO;2.
Rivalenti, G., Mazzucchelli, M., 2000. Interaction of mantle derived magmas and crust in the IVZ and the Ivrea mantle peridotites. In: Ranalli, G., Ricci, C.A., Trommsdorff, V. (Eds.), Crust Mantle Interactions, pp. 153–198.
Rudnick, R.L., McDonough, W.F., Chappell, B.W., 1993. Carbonatite metasomatism in the northern Tanzanian mantle: petrographic and geochemical characteristics. Earth Planet. Sci. Lett. 114, 463–475.
Sapienza, G.T., Scambelluri, M., Braga, R., 2009. Dolomite-bearing orogenic garnet peridotites witness fluid-mediated carbon recycling in a mantle wedge (Ulten Zone, Eastern Alps, Italy). Contrib. to Mineral. Petrol 158, 401–420.

Scambelluri, M., Hermann, J., Morten, L., Rampone, E., 2006. Melt- versus fluid-induced metasomatism in spinel to garnet wedge peridotites (Ulten Zone, Eastern Italian Alps): Clues from trace element and Li abundances. Contrib. to Mineral. Petrol. 151, 372–394. https://doi.org/10.1007/s00410-006-0064-9.

Scambelluri, M., Pettke, T., Cannaò, E., 2015. Fluid-related inclusions in Alpine high-pressure peridotite reveal trace element recycling during subduction-zone dehydration of serpentinized mantle (Cima di Gagnone, Swiss Alps). Earth Planet. Sci. Lett. 429, 45–59. https://doi.org/10.1016/j.epsl.2015.07.060.

Schauble, E.A., 2004. Fractionation Theory to New Systems. Rev. Min. Geochem. 55, 65–111.

Selverstone, J., Sharp, Z.D., 2011. Chlorine isotope evidence for multicomponent mantle metasomatism in the Ivrea Zone. Earth Planet. Sci. Lett. 310, 429–440. https://doi.org/10.1016/j.epsl.2011.08.034.

Shaw, D.M., 1970. Trace element fractionation during anatexis. Geochim. Cosmochim. Acta 34, 287–243.

Shervais, J., 1979. Thermal emplacement model for the Alpine lherzolite massif at Balmuccia, Italy. J. Petrol. 20, 795–820.

Shervais, J.W., Mukasa, S.B., 1991. The balmuccia orogenic lherzolite massif, Italy. J. Petrol. Special-vo 155–174. https://doi.org/10.1093/petrology/Special_Volume.2.155.

Sossi, P.A., Debret, B., 2021. The role of redox processes in determining the iron isotope compositions of minerals, melts and fluids. In: Moretti, R., Neuville, D.R. (Eds.), Magma Redox Geochemistry. John Wiley & Sons, Inc., pp. 303–330

Sossi, P.A., O'Neill, H.S.C., 2017. The effect of bonding environment on iron isotope fractionation between minerals at high temperature. Geochim. Cosmochim. Acta 196, 121–143. https://doi.org/10.1016/j.gca.2016.09.017.

Sossi, P.A., Halverson, G.P., Nebel, O., Eggins, S.M., 2015. Combined separation of Cu, Fe and Zn from rock matrices and improved analytical protocols for stable isotope determination. Geostand. Geoanalytical Res. 39, 129–149. https://doi.org/10.1111/j.1751-908X.2014.00298.x.

Sossi, P.A., Nebel, O., Foden, J., 2016. Iron isotope systematics in planetary reservoirs. Earth Planet. Sci. Lett. 1, 1–14. https://doi.org/10.1016/j.epsl.2016.07.032.

Sossi, P.A., Nebel, O., O'Neill, H.S.C., Moynier, F., 2018. Zinc isotope composition of the Earth and its behaviour during planetary accretion. Chem. Geol. 477, 73–84. https://doi.org/10.1016/j.chemgeo.2017.12.006.

Su, B.-X., Teng, F.-Z., Hu, Y., Shi, R.-D., Zhou, M.-F., Zhu, B., Liu, F., Gong, X.-H., Huang, Q.-S., Xiao, Y., others, 2015. Iron and magnesium isotope fractionation in oceanic lithosphere and sub-arc mantle: Perspectives from ophiolites. Earth Planet. Sci. Lett. 430, 523–532.

Syracuse, E.M., van Keken, P.E., Abers, G.A., Suetsugu, D., Bina, C., Inoue, T., Wiens, D., Jellinek, M., 2010. The global range of subduction zone thermal models. Phys. Earth Planet. Inter. 183, 73–90. https://doi.org/10.1016/j.pepi.2010.02.004.

Telus, M., Dauphas, N., Moynier, F., Tissot, F.L.H., Teng, F.Z., Nabelek, P.I., Craddock, P. R., Groat, L.A., 2012. Iron, zinc, magnesium and uranium isotopic fractionation during continental crust differentiation: The tale from migmatites, granitoids, and pegmatites. Geochim. Cosmochim. Acta 97, 247–265. https://doi.org/10.1016/j.gca.2012.08.024.

Teng, F.Z., Dauphas, N., Huang, S., Marty, B., 2013. Iron isotopic systematics of oceanic basalts. Geochim. Cosmochim. Acta 107, 12–26. https://doi.org/10.1016/j.gca.2012.12.027.

Tiraboschi, C., Mccammon, C., Rohrbach, A., Klemme, S., Berndt, J., 2023. ■ Preferential mobilisation of oxidised iron by slab-derived hydrous silicate melts. Geochemical Perspect. Lett. 24, 43–47.

Tommasi, A., Langone, A., Padrón-Navarta, J.A., Zanetti, A., Vauchez, A., 2017. Hydrous melts weaken the mantle, crystallization of pargasite and phlogopite does not: Insights from a petrostructural study of the Finero peridotites, southern Alps. Earth Planet. Sci. Lett. 477, 59–72. https://doi.org/10.1016/j.epsl.2017.08.015.

Turner, S., Williams, H., Piazolo, S., Blichert-Toft, J., Gerdes, M., Adam, J., Liu, X.M., Schaefer, B., Maury, R., 2018. Sub-arc xenolith Fe-Li-Pb isotopes and textures tell tales of their journey through the mantle wedge and crust. Geology 46, 947–950. https://doi.org/10.1130/G45359.1.

Walter, M., 1998. Melting of garnet peridotite and the origin of komatiite and depleted lithosphere. J. Petrol. 39, 29–60.

Walter, M.J., 2003. Melt Extraction and Compositional Variability in Mantle Lithosphere. Treatise on Geochemistry 2–9, 363–394. https://doi.org/10.1016/B0-08-043751-6/02008-9.

Wang, Z.Z., Liu, S.A., Liu, J., Huang, J., Xiao, Y., Chu, Z.Y., Zhao, X.M., Tang, L., 2017. Zinc isotope fractionation during mantle melting and constraints on the Zn isotope composition of Earth's upper mantle. Geochim. Cosmochim. Acta 198, 151–167. https://doi.org/10.1016/j.gca.2016.11.014.

Weyer, S., Ionov, D.A., 2007. Partial melting and melt percolation in the mantle: the message from Fe isotopes. Earth Planet. Sci. Lett. 259, 119–133. https://doi.org/10.1016/j.epsl.2007.04.033.

Williams, H.M., Bizimis, M., 2014. Iron isotope tracing of mantle heterogeneity within the source regions of oceanic basalts. Earth Planet. Sci. Lett. 404, 396–407. https://doi.org/10.1016/j.epsl.2014.07.033.

Williams, H.M., McCammon, C.A., Peslier, A.H., Halliday, A.N., Teutsch, N., Levasseur, S., Burg, J.P., 2004. Iron isotope fractionation and the oxygen fugacity of the mantle. Science (80-.) 304, 1656–1659. https://doi.org/10.1126/science.1095679.

Williams, H.M., Peslier, A.H., McCammon, C., Halliday, A.N., Levasseur, S., Teutsch, N., Burg, J.-P., 2005. Systematic iron isotope variations in mantle rocks and minerals: the effects of partial melting and oxygen fugacity. Earth Planet. Sci. Lett. 235, 435–452.

Wiser, N.M., Wood, B.J., 1991. Experimental determination of activities in Fe-Mg olivine at 1400 K. Contrib. Mineral. Petrol. 108, 146–153. https://doi.org/10.1007/BF00307333.

Wood, B.J., 1990. An experimental test of the spinel peridotite oxygen barometer. J. Geophys. Res. Solid Earth 95, 15845–15851. https://doi.org/10.1029/JB095iB10p15845.

Woodland, A.B., Koch, M., 2003. Variation in oxygen fugacity with depth in the upper mantle beneath the Kaapvaal craton. Earth Planet. Sci. Lett. 214, 295–310. https://doi.org/10.1016/S0012-821X(03)00379-0.

Woodland, A.B., Kornprobst, J., Wood, B.J., 1992. Oxygen Thermobarometry of Orogenic Lherzolite Massifs. J. Petrol. 33, 203–230. https://doi.org/10.1093/petrology/33.1.203.

Yan, S., Niu, H.-C., Zhao, Z., Li, N., Yang, W., Zhou, R., An, Y., Huang, F., 2024. Extremely low $δ$56Fe in arc tholeiites linked to ferrocarbonate recycling: implications for Fe enrichment in the Awulale Arc, Central Asia. Bulletin 136, 184–200.

Zanetti, A., Mazzucchelli, M., Rivalenti, G., Vannucci, R., 1999. The Finero phlogopite-peridotite massif: An example of subduction-related metasomatism. Contrib. Mineral. Petrol. 134, 107–122. https://doi.org/10.1007/s004100050472.

Zhang, R.Y., Liou, J.G., Yang, J.S., Yui, T.F., 2000. Petrochemical constraints for dual origin of garnet peridotites from the Dabie-Sulu UHP terrane, eastern-Central China. J. Metam. Geol. 18, 149–166. https://doi.org/10.1046/j.1525-1314.2000.00248.x.

Zhang, R.Y., Li, T., Rumble, D., Yui, T.F., Li, L., Yang, J.S., Pan, Y., Liou, J.G., 2007. Multiple metasomatism in Sulu ultrahigh-P garnet peridotite constrained by petrological and geochemical investigations. J. Metam. Geol. 25, 149–164. https://doi.org/10.1111/j.1525-1314.2006.00683.x.

Zhang, L., Sun, W., Zhang, Z., An, Y., Liu, F., 2019. Iron isotopic composition of supra-subduction zone ophiolitic peridotite from northern Tibet. Geochim. Cosmochim. Acta 258, 274–289.

Zhao, X.-M., Zhang, H.-F., Zhu, X.-K., Zhu, B., Cao, H., 2015. Effects of melt percolation on iron isotopic variation in peridotites from Yangyuan, North China Craton. Chem. Geol. 401, 96–110.

Zhao, X., Zhang, H., Zhu, X., Tang, S., Yan, B., 2012. Iron isotope evidence for multistage melt–peridotite interactions in the lithospheric mantle of eastern China. Chem. Geol. 292, 127–139.